arXiv:1403.6891v1 [astro-ph.SR] 26 Mar 2014

C/O Ratios of Stars with Transiting Hot Jupiter Exoplanets *,+

Johanna K. Teske[1], Katia Cunha[1,2], Verne V. Smith[3], Simon C. Schuler[4], Caitlin A. Griffith[5]

ABSTRACT

The relative abundances of carbon and oxygen have long been recognized as fundamental diagnostics of stellar chemical evolution. Now, the growing number of exoplanet observations enable estimation of these elements in exoplanetary atmospheres. In hot Jupiters, the C/O ratio affects the partitioning of carbon in the major observable molecules, making these elements diagnostic of temperature structure and composition. Here we present measurements of carbon and oxygen abundances in 16 stars that host transiting hot Jupiter exoplanets, and compare our C/O ratios to those measured in larger samples of host stars, as well as those estimated for the corresponding exoplanet atmospheres. With standard stellar abundance analysis we derive stellar parameters as well as [C/H] and [O/H] from multiple abundance indicators, including synthesis fitting of the [O I] 6300 Å line and NLTE corrections for the O I triplet. Our results, in agreement with recent suggestions, indicate that previously-measured exoplanet host star C/O ratios may have been overestimated. The mean transiting exoplanet host star C/O ratio from this sample is 0.54 ($C/O_{\odot}$=0.54), versus previously-measured $C/O_{\rm host\ star}$ means of ∼0.65-0.75. We also observe the increase in C/O with [Fe/H] expected for all stars based on Galactic chemical evolution; a linear fit to our results falls slightly below that of other exoplanet host stars studies but has a similar slope. Though the C/O ratios of even the most-observed exoplanets are still uncertain, the more precise abundance analysis possible right now for their host stars can help constrain these planets' formation environments and current compositions.

*Based on data collected at Subaru Telescope, which is operated by the National Astronomical Observatory of Japan.

+Some of the data presented herein were obtained at the W.M. Keck Observatory, which is operated as a scientific partnership among the California Institute of Technology, the University of California and the National Aeronautics and Space Administration. The Observatory was made possible by the generous financial support of the W.M. Keck Foundation.

[1]Steward Observatory, University of Arizona, Tucson, AZ, 85721, USA; email: jteske@as.arizona.edu

[2]Observatório Nacional, Rua General José Cristino, 77, 20921-400, São Cristóvão, Rio de Janeiro, RJ, Brazil

[3]National Optical Astronomy Observatory, 950 North Cherry Avenue, Tucson, AZ 85719, USA

[4]University of Tampa, 401 W. Kennedy Blvd., Tampa, FL 33606, USA

[5]Lunar and Planetary Laboratory, University of Arizona, Tucson, AZ, 85721, USA

Subject headings: planets and satellites: formation — stars: abundances — stars: atmospheres

1. Introduction

To date, the most statistically significant trend in host star abundances pertains to metallicity. Stars hosting giant, close-in planets have higher metallicities (measured as [Fe/H][1]) than stars without detected giant planets (e.g., Gonzalez 1998 & 2001; Santos et al. 2004; Fischer & Valenti 2005; Ghezzi et al. 2010). Statistical studies of dwarf stars hosting planets indicate a metallicity enhancement of ∼0.15 dex for stars with giant planets and a 99.9994% probability that stars with/without giant planets are drawn from different parent populations (Buchhave et al. 2012; Ghezzi et al. 2010). However, the host star metallicity trend is weaker for Neptune-sized planets – the difference in the mean [Fe/H] of Jovian-mass hosts versus Neptunian-mass hosts is ∼0.10 dex, with the Neptune-mass hosts showing lower [Fe/H] values (e.g., Ghezzi et al. 2010). Smaller planet ($R_P \leq 4\ R_\oplus$) host stars from the *Kepler* sample show no metallicity enhancement, and have a flatter distribution of metallicities, though roughly peaked at solar. These smaller planet host stars have a probability between 0.98 and 0.9996 of originating from a different parent population as larger planet host stars from *Kepler* (Buchhave et al. 2012; Everett et al. 2013).

Looking beyond the correlation between planet size and stellar metallicity, several studies have searched for other trends between planet parameters and host star abundances indicative of planet formation conditions. Meléndez et al. (2009) find through abundance analyses of 11 solar "twins" that the Sun is deficient by ∼20% in refractory elements, which have condensation temperatures $T_c \gtrsim 900$ K, relative to volatile elements when compared to other solar twins. This trend of decreasing refractory elemental abundances as a function of T_c is suggested to be a signature of terrestrial planet formation – the "missing" refractory elements from the stellar photosphere are incorporated into rocky planets (Meléndez et al. 2009). However, subsequent studies of similar precision measurements of solar analogs (González Hernández et al. 2010; González Hernández et al. 2013) and stars with planets (Schuler et al. 2011a & 2011b) across a range of T_c show that the abundance patterns of stars with and without planets are not significantly different, or may be indistinguishable from Galactic chemical evolution effects. New evidence from Jupiter- and Neptune-sized planet host stars that are more metal-rich, or warmer than the Sun and have less massive convective envelopes, indicates that the depletion signature may depend on the stellar convective envelope size at the time of planet formation, and thus the timescale of disk dispersal around different types of stars (Ramírez et al. 2013)

The growing number of transiting and directly-imaged exoplanet observations enable estimates

[1][X/H]=log$N$(X) - log$N$(X)$_\odot$, where log$N$(X)=log$N$(X/H)+12

of elemental and molecular abundances in the atmospheres of the planets themselves. The *Hubble Space Telescope* and *Spitzer Space Telescope*, aided by multiple ground-based facilities, have detected the most abundant molecules (H_2O, CO, CH_4, CO_2) in the atmospheres of several of the brightest transiting planets (e.g., Tinetti et al. 2007; Swain et al. 2008, 2009ab; Snellen et al. 2010; Beaulieu et al. 2010). Ground-based observatories have made similar strides in studying the molecular properties of a handful of directly imaged self-luminous exoplanets (e.g., Marois et al. 2008; Barman et al. 2011ab; Skemer et al. 2012, 2013; Konopacky et al. 2013; Janson et al. 2013). The differences and trends between the elemental compositions of host star and exoplanet atmospheres provide clues about the formation and evolution processes of planetary systems.

1.1. The Role of Carbon and Oxygen

Carbon and oxygen are important players in the composition of stars and planets, as the third and fourth most abundant elements in the universe. The measurement of C and O in stars, especially with respect to iron, which is produced in both Type Ia and Type II supernovae, serves as a fundamental diagnostic of the chemical enrichment history of the Galaxy. The impact of massive stars' Type II supernovae, and thus the major oxygen contributor, lessens with time and increasing metallicity as the influence of low- and intermediate-mass stars' carbon contribution grows. Measuring C and O in exoplanets is diagnostic of current atmospheric composition and temperature structure: the atmospheric C/O ratio[2] affects the molecular composition, and hence observed spectral signatures, through thermochemial equilibrium partitioning of carbon in CO, CH_4, and CO_2.

The C/O ratio can also reflect where in the protoplanetary disk a planet formed, as well as subsequent migration and evolution (e.g., Stevenson & Lunine 1988; Gaidos 2000; Ciesla & Cuzzi 2006; Öberg et al. 2011). Theories of planet formation describe how close-in giant planets form in the outer protoplanetary disk , where icy planetesimals coalesce into a core, which accretes gas and migrates inwards (e.g., Pollack et al. 1996; Owen et al. 1999; Ida & Lin 2004b). The main molecular reservoirs of C and O have different condensation temperatures (T_c), so their relative amounts vary at different temperatures and disk radii, as do the amounts of these molecules in gas or solid form (Öberg et al. 2011). Gas and grains also move differently in the disk with time, as grains grow and decouple from the gas, sequestering solid material beyond the "ice" lines of different molecules (e.g., Ciesla & Cuzzi 2006; Öberg et al. 2011). The C/O ratio of a planet therefore does not necessarily reflect the protoplanetary-disk-averaged C/O ratio, and instead may point towards localized concentrations/depletions of carbon- and oxygen-bearing molecules (Ciesla & Cuzzi 2006; Öberg et al. 2011; Najita et al. 2013).

[2]The C/O ratio – the ratio of carbon atom to oxygen atoms – is calculated in stellar abundance analysis as $C/O = N_C/N_O = 10^{\log N(C)}/10^{\log N(O)}$.

Many groups have performed stellar abundance analyses of exoplanet host stars in order to determine their physical parameters ($T_{\rm eff}$, log g, [Fe/H]) and chemical abundances, to further study the trends discussed above (e.g., Delgado Mena et al. 2010; Petigura & Marcy 2011; Brugamyer et al. 2011; Schuler et al. 2011ab; Nissen 2013). However, only a few transiting exoplanet host stars have published abundances other than [Fe/H] or the more generic [M/H] (e.g., HD 209458, Schuler et al. 2011a; WASP-12, Petigura & Marcy 2011; 55 Cnc, Bond et al. 2010 & Teske et al. 2013b; XO-2, Teske et al. 2013a).

Here we add to the small sample of transiting exoplanet host stars with measured abundances beyond [Fe/H], and the handful with measured C/O ratios. We report on sixteen transiting hot Jupiters hosts to investigate the extent to which we can relate host star compositions to those of their planets, and search for carbon-rich planet formation environments. The sample presented here contains the host stars of some of the most-observed exoplanets whose atmospheres can and are being modeled to constrain their C/O ratios (e.g., Madhusudhan 2012; Moses et al. 2013; Line et al. 2013). This work provides a step toward comparing specific host star and exoplanet atmospheres to search for the chemical effects of exoplanet formation.

2. Observations and Data Reduction

Our target list was chosen to include some of the best-studied hot Jupiter's host stars that are observable from the northern hemisphere, and to include a range of planet radii, masses, and orbital periods. All but three of the planetary hosts in this sample have at least the 3.6 μm, 4.5 μm, 5.8 μm, and 8.0 μm diagnostic measurements of secondary eclipse depth from the *Spitzer* Infrared Array Camera (IRAC) (Fazio et al. 2004). These data cover wavelengths with features of CH_4, CO, CO_2, and H_2O, which are the most abundanct oxygen and carbon molecules in hot Jupiter atmospheres. These measurements, in addition to *HST* and ground-based observations, are analyzed to infer the carbon and oxygen content in exoplanets (Moses et al. 2011, 2013; Lee et al. 2012; Madhusudhan 2012; Line et al. 2013), motivating our choice to target these host stars for C/O measurements. The planet orbiting HD 80606 has only 8.0 μm photometry, and the planets orbiting HAT-P-16 and WASP-32 have only 3.6 μm and 4.5 μm photometry, and CoRoT-2's planet is missing 5.8 μm photometry. We include these systems to increase the planet mass range in this sample to include members of the 2.8% of transiting planets with masses M$\times$sin$i$ > 3 M_J – HD 80606b is 3.94$\pm$0.11 M_J (Pont et al. 2009), HAT-P-16b is 4.19$\pm$0.09 M_J (Buchhave et al. 2010), and WASP-32b is 3.60$\pm$0.07 M_J (Maxted et al. 2010), and CoRoT-2b is 3.47 $\pm$0.22 M_J (Gillon et al. 2010).

There are three sources of observations for this project: the High Dispersion Spectrograph (HDS; Noguchi et al. 2002) on the 8.2-m Subaru Telescope at Mauna Kea Observatory, the High Resolution Echelle Spectrometer (HIRES; Vogt et al. 1994) at the Keck I Telescope, and the Keck/HIRES archive. All observations are logged in Table 1, and the platform configurations are detailed in Table 2. To facilitate a differential abundance analysis of these stars with respect

to the Sun (as indicated by the bracket notation), spectra of the Sun as reflected moonlight were taken at Subaru/HDS, and as reflected light from Vesta at Keck/HIRES (PID N014Hr; PI Marcy).

The HDS raw data were overscan-corrected, bias-subtracted, scattered-light subtracted, flat-fielded, extracted, and wavelength calibrated using standard techniques within the IRAF[3] software package using five bias frames, 20 flat fields, and thorium argon (ThAr) comparison lamp frames. All HIRES data were subject to a similar reduction procedure within the MAKEE pipeline[4] using corresponding bias (∼3), flat (∼30), ThAr, and trace star frames. Multiple exposures of single targets were then summed in IRAF.

We also obtained Keck/HIRES archive spectra of four targets that we originally observed with Subaru/HDS. The Subaru/HDS spectra were contaminated by atmospheric emission around the [O I] 6300 Å line, preventing a secure measurement of [O/H]; the O I triplet at ∼7775 Å was outside the Subaru/HDS wavelength coverage. Thus the Keck/HIRES archival data were used to verify the carbon abundance derived from the Subaru/HDS data, and to measure the oxygen abundance as described below. The four targets for which we obtained archival data are HAT-P-7 (PID A285Hr; PI Bakos; August 2008), TrES-3 (PID C290Hr; PI Herczeg; June 2008), HD 189733 (PID A259Hr; PI Winn; August 2006), and HD 149026 (PID N59H; PI Marcy; June 2005).

3. Derivation of Stellar Parameters and Abundances

We determine stellar parameters ($T_{\rm eff}$, log g, microturbulence [ξ]) and elemental abundances of Fe, C, Ni, and O following the procedures in Schuler et al. (2011a) and Teske et al. (2013a). Briefly, the strength and shape of absorption lines in stellar spectra depend on the formation environment (temperature, electron pressure) and the number and excitations state of absorbers themselves and thus their atomic constants. Thus one uses measurements from abundant, unblended lines in multiple ionization states – typically Fe – to determine the stellar environment in which the observed line strengths form, in an interative manner. The "best" stellar model parameters – effective temperature, microturbulent velocity, log g, and [Fe/H] – results from fulfilling excitation equilibrium such that the [Fe/H] values derived from the Fe I lines do not show any correlation with the lower excitation potential of the lines (χ), ionization equilibrium such that averaged abundances from Fe I and Fe II lines are equal, and ensuring that Fe I lines of all different equilvalent widths yield consisten abundances.

Specifically, the Fe lines in this analysis are the same as in Teske et al. (2013ab). The final Fe line list contains 56 Fe I and 10 Fe II lines, although not every Fe line is measureable in every star in the sample. Lower excitation potentials and transition probabilities for the Fe lines are from

[3]IRAF is distributed by the National Optical Astronomy Observatory, which is operated by the Association of Universities for Research in Astronomy, Inc., under cooperative agreement with the National Science Foundation.

[4]www.astro.caltech.edu/ tb/makee/

the Vienna Atomic Line Database (VALD; Piskunov et al. 1995; Kupka et al. 1999; Ryabchikova et al. 1999).

Abundances of Fe, C, and Ni are derived from equivalent width (EW) measurements of spectral lines in each target individually (sample Subaru/HDS spectra are shown in Fig. 1). The EW measurements are performed with the goal of mitigating errors of the fit – we use a Gaussian profile to fit most lines, though some strong lines (EW≥90 mÅ) are fit with a Voigt profile to account for the broader wings of the line at the continuum, and some weaker lines are fit with a Simpson's Rule approximation. The lines of the host stars are fit with either the one-dimensional spectrum analysis package SPECTRE (Fitzpatrick & Sneden 1987) or the 'splot' task in IRAF. The solar spectra corresponding to each target used to derive differential abundances were fit with the same package as the target, e.g., where we use EW measurements from SPECTRE, we use corresponding EW measurements from SPECTRE of the Sun in our analysis. The abundances are then determined with an updated version of the local thermodynamic equilibrium (LTE) spectral analysis code MOOG (Sneden 1973), with model atmospheres interpolated from the Kurucz ATLAS9 grids[5]. For oxygen, we use the spectral synthesis method of matching a set of trial synthetic spectra to the observed spectrum derive the abundance from the blended [O I] line at $\lambda = 6300.3$ Å (see Fig. 2).

Initial values of $T_{\rm eff}$, log g, ξ, and [Fe/H] from the literature serve as our starting values in the iterative process of meeting the criteria outlined above. Prior to this iterative scheme, for each target's EW measurements we ensure no correlation between χ and the EWs of the Fe I lines analyzed, as unique solutions for $T_{\rm eff}$ and ξ are only possible if there is no such initial correlation. The log$N$(Fe) values for the Sun are determined from the solar spectrum with a solar Kurucz model with $T_{\rm eff}$=5777, log g=4.4 [Fe/H]=0.00, and ξ=1.38, and log$N$(Fe) values of the target stars are normalized to solar values on a line-by-line basis. The final [Fe/H] results from averaging the abundances derived from the individual Fe I and Fe II lines.

Uncertanties in the derived stellar parameters are calculated as detailed in Teske et al. (2013a). In Table 3 we list the final derived stellar parameters and their 1σ uncertainties for each target, as well as the derived [Fe I/H] and [Fe II/H], the number of lines used in our analysis, and the uncertainy in the mean (σ_μ[6]).

3.1. Stellar Abundances of Ni, C, and O

A similar procedure as that used for the Fe lines is used to identify and select lines for Ni and C, with the same line lists as Teske et al. (2013ab), which include 5 lines for carbon and 20 lines for nickel, though not every line was measureable in every star in our sample. The C and Ni

[5]See http://kurucz.harvard.edu/grids.html

[6]$\sigma_\mu = \sigma/\sqrt{N-1}$, where σ is the standard deviation of the derived abundances and N is the number of lines used to derive the abundance.

abundances are determined through standard EW analysis procedures with MOOG and the adopted stellar model for each target. The wavelength, χ, log gf, measured EW, and resulting abundances for the carbon lines are listed in Table 4 for a sample of the targets. All lines parameters, equivalent widths, and resulting abundances are available in the full online version of Table 4.

We favor the two bluest C I lines (5052 Å and 5380 Å) in our analysis because they arise from the lowest energy levels considered here and have negligible non-LTE (NLTE) corrections ($\leq$0.05; Asplund et al. 2005; Takeda & Honda 2005; Caffau et al. 2010). The log$N$(C)$_\odot$ values we derive with our EW measurements are a good match (within $\leq$0.03 dex) to the log$N$(C)$_\odot$ values derived by Caffau et al. (2010) from these lines using 3D hydrodynamical simulations of the Sun. The remaining three C I lines arise from higher energy levels, potentially making them more susceptible to NLTE effects (Asplund 2005), although Asplund et al. (2005) find NLTE corrections for these lines in the Sun are comparable to those for the bluer C I lines. In cases where we find discrepant (larger) carbon abundances from the redder C I lines, we base our [C/H] measurement on the two bluest C I lines.

In HAT-P-7, TrES-3, HD 149026, and HD 189733, [O/H] is not measurable with the Subaru/HDS data because the [O I] 6300 Å is contaminated by atmospheric emission and the wavelength coverage ends blueward of the O I triplet. The oxygen abundances of these four targets are instead measured from Keck/HIRES archive data (detailed below). In these cases the stellar parameters and [Ni/H] derived from the Subaru/HDS data are carried through the analysis, but [C/H] is remeasured in the Keck/HIRES data so that the C/O ratio originates completely from one data source. In all four cases the [C/H]$_{\rm HIRES}$ value is equal to the [C/H]$_{\rm HDS}$ value within errors, with the differences all $\leq$0.04 dex, giving confidence to this method.

3.1.1. Oxygen

The oxygen abundances of the targets in our sample are determined from two indicators, the forbidden [O I] line at λ = 6300.3 Å and the O I triplet at 7771-7775 Å, depending on what data are available. For seven of the thirteen (including XO-2S) targets, the oxygen abundance is derived solely from the Subaru/HDS data and the [O I] line, which is well-described by LTE (e.g., Takeda 2003). We adopt the Storey & Zeippen (2000) log gf =-9.717 value, based on their forbidden transition probability calculations including both relativistically-corrected magnetic dipole and electric quadruopole contributions. However, the 6300.3 Å feature is blended with a Ni I line composed of two isotopic components, with log gf(^{60}Ni)=-2.695 and log gf(^{58}Ni)=-2.275 (Johansson et al. 2003; Bensby et al. 2004). In the Sun, nickel accounts for ∼30-40% of the [O I] absorption line depth (Caffau et al. 2008; 2013). Therefore, in determining [O/H] from this line, we account for the nickel component by measuring [Ni/H] directly from each target's spectrum as described above and appropriately scaling the strength of the blend component due to nickel. We also test for potential blending in the 6300.3 Å [O I] line with another, much weaker, CN line (Davis & Phillips 1963; Sneden & Lambert 1982) by fixing the carbon abundance to our measured

[C/H] value and remeasuring the 6300 Å line oxygen abundance. Except in the cases of XO-2N and XO-2S (Teske et al. 2013b), our resulting oxygen abundances do not change significantly ($\leq$0.02 log$N$(O)) by fixing the carbon abundance.

The free parameters in our synthesis fits are the continuum normalization, wavelength shift, line broadening, and oxygen abundance; we use our measured Ni and C abundances for each star, and N scaled from solar based on the measured [Fe/H] of each star. We also checked our synthesis results with the "blends" driver in MOOG, which accounts for contributions from additional lines to the primary element with a user-provided line list including these blending lines and corresponding blending species abundances. In Table 4 we list the measured EWs serving as input for our check with the "blends" driver and absolute abundances as determined from synthesis fitting of the [O I] line for a sample of the targets.

For the spectra in which the Subaru/HDS [O I] 6300.3 Å is tellurically contaminated (HAT-P-7, TrES-3, HD 149026, and HD 189733) the even weaker [O I] 6363.79 Å line is not distinguishable from noise, and the O I triplet at 7771-7775 Å is not covered. However, the public data retrieved from the Keck/HIRES archive do include the triplet at 7771-7775 Å and, in some cases, also display clean (not tellurically contaminated) [O I] 6300 Å lines. In TrES-3, the data beyond $\sim$7050 Å are contaminated due to saturated ThAr lamp calibrations; fortunately in this case the [O I] 6300 Å is measurable in the Keck/HIRES data. We also obtained our own Keck/HIRES data for HAT-P-1, HAT-P-16, and WASP-32, and use the [O I] 6300 Å and O I triplet lines to derive oxygen abundances for these targets, as well as the stellar parameters and the [C/H] and [Ni/H] values.

In solar-type stars, the O I triplet lines at 7771.94 Å (χ=9.15 eV, log gf=0.369; Hibbert et al. 1991), 7774 Å (χ=9.15 eV, log gf=0.223; Hibbert et al. 1991), and 7775.4 Å (χ=9.15 eV,log gf= 0.001; Hibbert et al. 1991) are prominent and suffer less from blending with other lines, and are therefore conducive to direct EW measurement (Table 4). These lines are known to suffer from NLTE effects, detailed in Kiselman (1993; 2001) and Gratton et al. (1999), and several groups have derived NLTE corrections from statistical equilibrium calculations for varying stellar parameters. For comparison, as in Teske et al. (2013a), we apply NLTE corrections to the triplet abundances from three sources: Takeda (2003), Ramírez et al. (2007), and Fabbian et al. (2009) (Table 5). The differences in methodology applied by each of these sources to determine NLTE corrections is detailed in Teske et al. (2013a), who also note that the NLTE corrections from different sources give overlapping results.

The validity of using such NLTE corrections for cool ($T_{\rm eff}$ $\lesssim$5400 K) stars is questionable, as discussed in Teske et al. (2013a). They ultimately choose not to include the NLTE-corrected O I triplet abundances for the cool, metal-rich star 55 Cnc, instead relying on the averaged [O I] 6363.79 Å and LTE O I triplet abundances. In the spectra presented here, which are of lower S/N than the 55 Cnc data presented in Teske et al. (2013a), the [O I] 6363.79 Å line is not detected. Thus, in the case of stars with $T_{\rm eff}$ $\lesssim$5400 K and for which we have Keck/HIRES data with wavelength coverage including the O I triplet, we adopt the average of the [O I] 6300 Å and LTE O I triplet

abundances. For warmer stars in which both the [O I] 6300 Å and O I triplet lines are measurable, we adopt the average of the [O I] 6300 Å and the three NLTE-corrected O I triplet abundances. In all cases the [O I] 6300 Å- and O I triplet-derived (whether LTE or NLTE) abundances match within the uncertainties.

Table 6 lists the final averaged [O/H] values for each target, along with [C/H] and the resulting C/O ratio. These C/O ratios are calculated with the prescription $\log N_{\rm target}({\rm O})$=derived $[{\rm O/H}]_{\rm target}+\log N_{\odot}({\rm O})$ and $\log N_{\rm target}({\rm C})$=derived $[{\rm C/H}]_{\rm target}+\log N_{\odot}({\rm C})$, where $\log N_{\odot}({\rm O})$=8.66 and $\log N_{\odot}({\rm C})$=8.39 (solar values from Asplund et al. 2005). This table also shows the measured [Ni/H] abundances for each target, which are used in the derivation of [O/H] from the [O I] 6300 Å line as described above.

3.2. Abundance Uncertanties

The uncertainties in the derived elemental abundances include the errors in the adopted stellar parameters ($T_{\rm eff}$, log g, and ξ) and the dispersion in the abundances derived from different absorption lines for the element, as the final adopted abundance is an average of these lines. To determine the uncertainty due to the stellar parameters, the sensitivity of the abundance to each parameter was calculated for changes of ±150 K in $T_{\rm eff}$, ±0.25 dex in log g, and ±0.30km s^{-1} in ξ. These calculated abundance sensitivities for two targets, WASP-12 and HAT-P-1, are shown as an example in Table 7. The final uncertainty due to each parameter is then the product of this sensitivity and the corresponding scaled parameter uncertainty, as described in Teske et al. 2013a. The dispersion in the abundances derived from different lines is parameterized with the uncertainty in the mean, σ_{μ} , for the abundances derived from the averaging of multiple lines. Then the total internal uncertainty for each abundance ($\sigma_{\rm tot}$) is the quadratic sum of the individual parameter uncertainties and σ_{μ}.

In the case of the O I triplet, the error on $[{\rm O/H}]_{\rm NLTE}$ was calculated separately for each of the applied NLTE corrections, but as these errors are smaller than the error derived from the LTE measurement, the LTE errors are conservatively adopted. In the cases of more than one measurable oxygen abundance indicator, the errors associated with [O/H] reported in Table 6 are the errors from each oxygen abundance indicator ([O I] 6300 Å and LTE O I triplet) added in quadrature, unless otherwise noted. Similarly, the C/O ratio errors are the errors of [C/H] and [O/H] combined in quadrature.

4. Results and Discussion

Our final adopted stellar parameters and their 1σ uncertainties for each target are listed in Table 3, and the adopted elemental abundances and their 1σ uncertanties for each target are listed in Table 6. We compared our results to those of the catalog of Stars With ExoplanETs (SWEET-Cat), described in Santos et al. (2013), and those determined by Torres et al. (2012; T12). These two

references are comparable to ours in their analysis methods and samples (transiting exoplanet host stars). SWEET-Cat compiles sets of atmospheric parameters previously published in the literature and, whenever possible, derived using the same uniform methodology of Santos et al. (2004). The main sources of stellar parameters in SWEET-Cat for the targets in our sample are Santos et al. (2004), Ammler-von Eiff et al. (2009), and Mortier et al. (2013). SWEET-Cat reports $T_{\rm eff}$, [Fe/H], and log g for all of the targets in our sample of stars, and ξ for ten of the targets.

T12 compared the resulting $T_{\rm eff}$ and [Fe/H] from three different stellar analysis programs. They include stellar parameter classification (SPC; Buchhave et al. 2012), Spectroscopy Made Easy (SME; Valenti & Piskunov 1996), and MOOG, the latter of which we employ here. They also determine log g values, but do not report them, and v sin i values, which we do not determine in our work. T12 report final "averaged" $T_{\rm eff}$ and [Fe/H] values from all attempted analysis methods for thirteen of the stars in our sample, though MOOG-derived $T_{\rm eff}$ and [Fe/H] values are included in that average for only ten of the stars in our sample.

In all cases our derived [Fe/H] values are consistent with those of SWEET-Cat and T12-average, within uncertainties. The median Δ[Fe/H] (as in |ours - theirs|) values are 0.08 and 0.02 for SWEET-Cat and T12-average, respectively. The $T_{\rm eff}$ and log g values reported here also overlap within uncertainties the values reported in T12-average and those in SWEET-Cat in almost every case. The median Δlog g for SWEET-Cat is 0.17, and the median $\Delta T_{\rm eff}$ for SWEET-Cat and T12-average are 55 K and 41 K, respectively. In the two cases where $T_{\rm eff}$ does not overlap SWEET-Cat our values are cooler by 54 K (WASP-12) and 202 K (WASP-32). Two other sources (Brown et al. 2012; Maxted et al. 2010) report a very similar $T_{\rm eff}$ for WASP-32 as the (cooler) value derived here, and the results of Torres et al. (2012) for WASP-12 agree well with our $T_{\rm eff}$. In the three cases where log g does not overlap SWEET-Cat or T12-average our values differ by $\leq$0.04 dex.

4.1. Comparison to Previous Studies of C and O in Exoplanet Host Stars

This study focuses on transiting exoplanet host star elemental abundances, particularly their C/O ratios. No previous study of which we are aware has uniformly derived [C/H], [O/H], and C/O values for these stars. However, several studies have examined C/O ratios in non-transiting exoplanet host stars versus stars not known to host planets. [Any star designated as a "non-host" has the potential to harbor a smaller (undetected) planet; indeed, it may be the case that most stars have one or more small planets (e.g., Cassan et al. 2012).] Here we compare our results to these other host star C/O studies.

Bond et al. (2006) measure [C/H] in 136 G-type stars, 20 of which are exoplanet hosts, and Bond et al. (2008) measure [O/H] ratios in 118 F- and G-type stars stars, 27 of which are known exoplanet hosts. Line lists are not explicitly given for the measured C lines in Bond et al. (2006); Bond et al. (2008) use the high-excitation O I triplet at λ = 7771.9, 7774.2, and 7775.4 Å. Bond et al. (2010) also compiled C/O ratios derived from measurements in Ecuvillion et al. (2004) and

(2006). Ecuvillion et al. (2004) measures [C/H] from the two lowest excitation lines of carbon (5052.17 and 5380.34 Å), and Ecuvillion et al. (2006) measures [O/H] from the forbidden [O I] line at 6300.3 Å, the high-excitation O I triplet at $\lambda = 7774$ Å, and a set of 5 near-UV OH lines around 3100 Å. Both of the Ecuvillion studies and the Bond studies implement an analysis method similar to that performed here, with the spectral synthesis code MOOG and a grid of Kurucz (1993) ATLAS9 model atmospheres, although these studies do not derive the host star parameters ($T_{\rm eff}$, $\log g$, ξ, and [Fe/H]), only specific elemental abundance ratios. In the host star sample reported in Bond et al. (2010), 35% have C/O>0.8 (they did not specifically report any non-host stars); Bond et al. (2008) find 8% of host stars and 5% of non-host stars in their sample to have C/O>0.8.

Following the Bond et al. investigation, two larger studies of the C/O ratios of non-host stars versus host stars were conducted. Delgado Mena et al. (2010) measure carbon and oxygen in 100 host stars, along with 270 non-host stars, using the C I lines at 5052.17 Å and 5380.34 Å and the [O I] forbidden line at 6300.3 Å. They measure equivalent widths with the ARES program[7] (Sousa et al. 2007), and used MOOG and Kurucz ATLAS9 model atmospheres (Kurucz 1996) for abundance analysis. Delgado Mena et al. (2010) find 34% of their measured host stars have C/O>0.8, while in their non-host sample the fraction of stars with C/O>0.8 is 20%. Petigura & Marcy (2011) find carbon and oxygen abundances for 704 and 604 stars, respectively, but only 457 have reliable measurements for both elements that can be used to determine C/O ratios, 99 of which are exoplanet hosts. These authors measure the 6587 Å C I line for carbon and the [O I] line at 6300.3 Å for oxygen, and use the SME code with Kurucz (1992) stellar atmospheres for their abundance analysis. Petigura & Marcy (2011) find 34% of host stars in their sample have C/O>0.8, versus 27% of non-host stars in their sample with with C/O>0.8.

The goal of this paper is to investiage and constrain values of stellar host C/O ratios in systems with observed transiting giant planets, since transit spectroscopy potentially allows for determinations of the corresponding planetary C/O ratios. This goal is driven partially by the recent suggestion by Fortney (2012) that the C/O ratios of both host- and non-host stars in the studies noted above have been overestimated due to errors in the derived C/O ratios and the observed apparent frequency of carbon dwarf stars implied by these studies.

Nissen (2013) recently rederived the carbon and oxygen abundances for 33 of Delgado Mena et al. (2010)'s host stars that have additional ESO 2.2m FEROS spectra covering the O I triplet at 7774 Å, which was not originally used by Delgado Mena. He implements a differential analysis with respect to the Sun, with equivalent widths of C and O measured in IRAF with Gaussian profiles and abundances derived by matching the observed equivalent widths with those measured in plane parallel MARCS atmosphere models (Gustafsson et al. 2008) having the same stellar parameters as those published by Delgado Mena et al. (2010). Accounting for NLTE effects on the triplet line strengths by using the Fabbian et al. (2009) corrections, Nissen (2013) finds differences from Delgado Mena et al. (2010) in the derived oxygen abundances. This results in both a tighter

[7]The ARES code can be downloaded at http://www.astro.up.pt/sousasag/ares/.

correlation between [Fe/H] and C/O (Nissen finds C/O = 0.56+0.54[Fe/H] with an rms dispersion σ(C/O)=0.06), as well as a much smaller fraction of host stars with C/O>0.8 (only 1 out of 33).

The tight trend of increasing C/O with [Fe/H], e.g., Nissen (2013; as noted above), is indicative of the importance of overall Galactic chemical evolution in setting the fraction of dwarf stars that might be carbon rich. The increase in C/O with metallicity points to the importance of low- and intermediate-mass star carbon nucleosynthesis at later, more metal-rich times. The influence of mass-star Type II supernovae, the major oxygen contributors, is diluted with time as low- and intermediate-mass stars become more important, thus C/O increases. The fraction of "carbon-rich" (C/O $\geq$0.8) planet-hosting stars is thus expected to increase with increasing metallicity in the disk, with the Nissen trend indicating metallicities greater than [Fe/H]$\sim$0.4 might begin to have significant fractions of carbon-rich dwarf stars. All of the planet-hosting stellar samples discussed here have very few, if any, stars at these metallicites or higher.

This paper differs from the studies listed above because 1) the sample here is much smaller, being limited to only hosts of transiting exoplanets, and 2) only one non-host star is included (the binary companion XO-2S). In Figure 3 the host star abundances derived here, shown with red filled circles with error bars, for [C/H] and [O/H] versus [Fe/H] are compared to the results of the large samples of Delgado Mena et al. (2010), shown as gray asterisks for host stars and open squares for non-host stars, and Nissen (2013), shown as blue asterisks. All three studies define similar behaviors of [C/H] and [O/H] as a function of [Fe/H], with the carbon exhibiting larger slopes with iron relative to oxygen; this illustrates the increasing importance of carbon production from low- and intermediate-mass stars relative to massive stars with increasing chemical maturity.

The slopes of the trends in Figure 3 are all quite similar, with the Nissen (2013) trend exhibiting the smallest scatter about a linear fit. Using the results of this paper, linear trends are fit to both [C/H] and [O/H] versus [Fe/H] with the following results: [C/H] = 0.95[Fe/H] - 0.05 and [O/H] = 0.56[Fe/H] + 0.01. Excluding the apparently carbon-rich outlier HD 189733, these fits are [C/H] = 1.02[Fe/H] - 0.08 and [O/H] = 0.56[Fe/H] + 0.01; we refer to these fits without HD 189733 throughout the rest of the paper. Quantitatively, the C versus Fe slope is about twice as large (in dex) as that for O versus Fe based on the linear fits to the abundances derived here. The relation for carbon passes 0.08 dex below solar (i.e., at [Fe/H],[C/H]=0,0) while passing close to solar for oxygen, offset by only +0.01 dex.

Because of these even rather small offsets ($\sim$0.05-0.1 dex), the C/O ratios as a function of [Fe/H] might fall below solar as defined by our results for this particular sample of stars: an offset of -0.05 to -0.1 dex in [C/O] would correspond to an offset of 0.1 to 0.2 lower in a linear value of C/O. This does not necessarily correspond to simply errors in the analysis, but may reflect both fitting linear relations to our results, which are probably only approximate descriptions of the real Galactic disk relation, as well as there not being a universal trend of [C or O]/H versus [Fe/H]. The offsets here most probably reflect both uncertainties in the analysis (already discussed in Section 3.2) and intrinsic scatter in real Galactic disk populations that will map onto the sample of stars

analyzed here.

Figure 4 illustrates values of C/O versus [Fe/H] from this study, along with those values from Delgado Mena et al. (2010) and Nissen (2013). All three studies find a clear increase in C/O verus [Fe/H], which represents the signature of Galactic chemical evolution, as discussed previously. The relation in C/O in this work falls somewhat below those of the other two studies, but all three exhibit similar slopes. This similarity is born out by a quantitative comparison of C/O versus [Fe/H] between Nissen (2013) and this study. Nissen derived a linear fit of C/O = 0.54[Fe/H] + 0.56, while the same fit to the results here find C/O = 0.53[Fe/H] + 0.45. The adopted solar value in this study of C/O = 0.54 is larger by 0.09 than the value defined by the best-fit linear relation defined by our sample of stars and our results. Including the outlier HD 189733 in our linear fit results in C/O = 0.43[Fe/H] + 0.49, corresponding to a C/O ratio 0.05 smaller than the solar value of 0.54; including this outlier increases the scatter around the fit from 0.04 to 0.1. A linear difference of 0.09 corresponds to 0.08 dex for the solar-relative [C/O], which is comparable to the repsective offsets of -0.08 dex and +0.01 dex in the [C/H] and [O/H] relations.

Another way of investigating the inherent scatter within our results is to remove the linear best-fit from the values of C/O and look at the scatter about the fitted relation. When this is done the median residual scatter in C/O is ±0.04 , or 0.03 dex in [C/O]. This comparison of C/O versus [Fe/H] trends between Nissen (2013) and this study indicates that the derived slopes are very similar, but there remain small offsets in zero-point C/O of $\sim$ 0.10 - 0.15 caused by a combination of differences in (presumably) the stellar samples, the adopted solar C/O ratios (0.58 for Nissen and 0.54 for this study), as well as the abundance analysis, e.g., much of the offset is due to somewhat smaller values of [C/H] at our lower metallicity range.

The mean and standard deviation of the [C/H], [O/H], and C/O distributions from this study, as well as those from all the previous studies of host star carbon and oxygen abundances mentioned above, are listed in Table 8. The mean [C/H] of the transiting exoplanet hosts in this paper is less than the mean $[C/H]_{host}$ from the previous works, 0.14 in the five previous studies versus 0.08 found here. The mean [O/H] value found in our sample is the same as the mean $[O/H]_{host}$ from previous studies, 0.07. However, the standard deviations of $[C/H]_{transiting}$ and $[O/H]_{transiting}$ from this paper are large, 0.20 and 0.13, respectively, so any differences in our mean [C/H] and [O/H] values are to be viewed with caution. The mean C/O ratio of the transiting exoplant host stars in our sample is 0.54, with a standard deviation of 0.15, versus the mean from the previous papers of 0.71 with a standard deviation of 0.07. Therefore, the sample of carbon and oxygen abundance ratios for transiting exoplanet host stars presented here, while marginally consistent, are on average lower than those measured by other groups for non-transiting exoplanet host stars. Our measurements are more in line with the suggestions by Fortney (2012) and Nissen (2013) that prior studies overestimated C/O ratios; the mean C/O_{hosts} of Nissen is 0.63±0.12.

However, as noted by Fortney (2012), each previous study scales their C/O ratios based on different $\log N(C)_{\odot}$ and $\log N(O)_{\odot}$ values. Delgado Mena et al. (2010) list $\log N(C)_{\odot}$ and $\log N(O)_{\odot}$

as 8.56 and 8.74, respectively, resulting in $C/O_{\odot}$=0.66. These are also the values listed in Ecuvillion et al. (2004) and (2006), the quoted sources of Bond et al. (2010). Petigura & Marcy (2011) list $\log N(C)_{\odot}$ and $\log N(O)_{\odot}$ as 8.50 and 8.70, respectively, resulting in $C/O_{\odot}$=0.63. Nissen (2013)'s $C/O_{\odot}=10^{8.43}/10^{8.665}$=0.58. Figure 4 illustrates the different $C/O_{\odot}$ from Delgado Mena et al. (2010) and Nissen (2013). Accounting for the difference in $\log N(C)_{\odot}$ and $\log N(O)_{\odot}$ decreases the average C/O ratios from the other sources (from top to bottom) in Table 8 by ∼0.15, ∼0.13, ∼0.11, and ∼0.05, closer to the average C/O ratio we derive for our sample. Figure 4's right panel shows the C/O ratios of Delgado Mena et al. (2010) and Nissen (2013) along with those derived in this work, all on the same scale, illustrating how using different solar C and O absolute abundances changes the resulting C/O ratios. This underscores the caution, as mentioned in Fortney (2012) and Nissen (2013), required when directly comparing C/O ratios derived from different groups.

We now focus on the C/O ratios in each studied system to investigate possible links between host star C/O ratios with planetary and system properties.

4.2. Trends with $C/O_{\rm host\,star}$ versus Planetary Parameters

Presently there are two major observed trends relating stellar chemical composition to the presence of planets – hot Jupiter exoplanets are more often found around intrinsically higher-metallicity stars (e.g., Fischer & Valenti 2005), and the fraction of stars with giant planets increases with stellar mass (e.g., Johnson et al. 2010; Ghezzi et al. 2010; Gaidos et al. 2013). Measuring potential host stars' chemical abundance distributions may develop into a powerful tool for inferring the presence, or even specific type (size, orbit, composition), of exoplanets around different types of stars. This technique is of increasing importance in the context of large surveys that are discovering exoplanets, and targeted studies of unusual or potentially-habitable exoplanets.

In this study we explore whether the stellar C/O ratio has predictive power with respect to hot Jupiter properties, particularly the exoplanetary atmosphere compositions. Characteristic observations of the atmospheres of the exoplanets in this sample – the *Spitzer/IRAC* 3.6, 4.5, 5., and 8.0 μm secondary eclipse fluxes – as well as their physical properties like mass, radius, semi-major orbital axis, period, and equlibrium temperature were gathered from the NASA Exoplanet Archive[8] and compared to host star C/O ratios. By eye it appears that planet radius and planet equlibrium temperature may decrease with increasing $C/O_{\rm host\,star}$ (Fig.5), but these trends are dominated by one or two points and, once these points are removed, no significant trends with planet parameters are found. We also find weak negative correlations between each system's $C/O_{\rm hoststar}$ and planetary *Spitzer*/IRAC secondary eclipse fluxes (e.g., r ∼-0.4 to -0.6), but these correlations are not statistically significant (p >0.05).

This lack of trends between $C/O_{\rm host\,star}$ is perhaps not surprising. The hot Jupiter host stars

[8]http://exoplanetarchive.ipac.caltech.edu/

in this sample were chosen based on the amount of observational data that exists for their planets, and thus how "characterizable" their planets' atmospheres are, with the goal of directly comparing star and planet C/O ratios. No planetary or stellar parameters serve as "control variables" in this study, and our sample is actually diverse in both respects. The host stars span $5100 \lesssim T_{\rm eff} \lesssim 6470$ K, $-0.21 \lesssim$[Fe/H]$\lesssim 0.44$, and spectral types F6 through K1. The planets in our sample range in mass from ∼0.5-4.2 M_J, in period from ∼1.09-111 days (with the second longest being 4.5 days), in density from ∼0.2-8 g cm^{-3} (with the second most-dense being 3.4 g cm^{-3}), and in equilibrium temperature from ∼400-2500 K. That we do not find a significant correlation between $C/O_{\rm host\,star}$ and any of these planetary parameters implies that (1) our sample may yet be too small to reveal distinct trends, and/or (2) the influence of the host star C/O ratio is a more complex function of multiple parameters of the planet and/or its formation history.

While (1) is possible, (2) also seems likely and could result in the C/O ratio comparison between stars and planets serving a more interesting function. In protoplanetary disks, different condensation fronts due to temperature and the movement of gas and grains in the disk can change the relative ratios and/or of carbon and oxygen as compared to those in the parent star (Stevenson & Lunine 1988; Lodders 2010; Ciesla & Cuzzi 2006; Öberg et al. 2011). In particular, the enhancement or depletion of water and thus oxygen is sensitive to the size and migration of icy solids in the disk, so the C/O ratios of the inner and outer disk regions evolve with time and depend on both initial conditions and the efficiency with which solids grow to large sizes (Ciesla & Cuzzi 2006; Najita et al. 2013). Overall, the final $C/O_{\rm planet}$ does not necessarily reflect the $C/O_{\rm disk-average}$, and depends on the location and timescale of formation, how much of the atmosphere is accreted from gas versus solids, and how isolated the atmosphere is from mixing with core materials (Ciesla & Cuzzi 2006; Öberg et al. 2011). In our own solar system gas giant planets, oxygen is not well constrained because water, the major oxygen carrier, condenses deeper down in their cool ($T \leq 125$ K) atmospheres, out of the observable range of remote spectra (Madhusudhan 2012). However, carbon is known to be enhanced above solar by factors of ∼2-6, 6-11, 18-50, and 28-63 in Jupiter, Saturn, Uranus, and Neptune, respectively (Wong et al. 2008 and references therein). Thus, though the composition of the host star provides a good estimate of the system C/O ratio and the natal molecular cloud environment, differences between the host star and planetary C/O ratios may be common, and may be used to probe where and when in the disk the planet formed.

A third possibility is that the host star C/O ratio has no connection to the formation of planets and is not a useful metric for distinguishing planet types. However, theoretical results (e.g., Johnson et al. 2012; Ali-Dib et al. 2013) demonstrating the influence of the host star C/O ratio on the composition of protoplanetary disk, and recent observations (e.g., Najita et al. 2013; Favre et al. 2013) indicating that disks themselves likely have a range of C/O ratios which are related to other planet formation parameters (mass of the disk, grain growth and composition, etc.), suggest that C/O ratios of host stars do play a role, at some stage, in planet formation.

4.3. Carbon and Oxygen in Specific Exoplanet Systems

A small fraction of exoplanets, mostly hot Jupiters orbiting very close to their host stars, have been observed and analyzed with spectroscopy and photometry in the optical and near-infrared during primary transit (e.g., Madhusudhan & Seager 2009; Swain et al. 2008, 2013; Moses et al. 2011; Mandell et al. 2013) and/or secondary eclipse (e.g., Charbonneau et al. 2005, 2008; Knutson et al. 2008; Madhusudhan et al. 2011; Crossfield et al. 2012). Direct imaging of exoplanets in wider orbits (e.g., Marois et al. 2008 & 2010; Lagrange et al. 2009; Bailey et al. 2014) has also opened up for study a new population of self-luminous planets in Jovian-type orbits.

As discussed in the introduction, a gas giant planet's C/O ratio has important implications for its composition. At the temperatures and pressures characteristic of such atmospheres, a high C/O ratio ($\gtrsim$0.8) can significantly alter the temperature and chemistry structure by depleting the dominant opacity source H_2O and introducing new sources that are C-rich like CH_4, HCN, and/or other hydrocarbons. In thermochemical equilibrium, C/O>1 causes O to be confined mostly to CO, depleting H_2O and enhancing CH_4 versus what is expected in solar-abundance atmospheres ($C/O_\odot$=0.55±0.10; Asplund et al. 2009; Caffau et al. 2011), which have abundant H_2O and CO (Madhusudhan 2012; Moses et al. 2013). In carbon-rich atmospheres, the temperature controls how depleted the H_2O is compared to solar and the partitioning of carbon between CH_4 and CO, which in turn influences the oxygen balance between CO and H_2O (Madhusudhan 2012).

With the ability to constrain exoplanet atmosphere compositions (e.g., Madhusudhan 2012; Lee et al. 2012; Moses et al. 2013; Konopacky et al. 2013; Line et al. 2013), a logical next step towards determining the host star's influence on exoplanet formation is the direct comparison of the abundance ratios of star/planet pairs.

4.3.1. WASP-12

For WASP-12b, one of the brightest transiting exoplanets, the comparison between host star and planet composition has already begun (Madhusudhan et al. 2011; Madhusudhan 2012; Petigura & Marcy 2011; Crossfield et al. 2012; Swain et al. 2013; Copperwheat et al. 2013; Sing et al. 2013). The host star is found in this work to have [Fe/H] = 0.06±0.08 and C/O=0.48±0.08. We note that this metallicity differs significantly from the [M/H]= $0.30^{+0.05}_{-0.10}$ reported by Hebb et al. (2009) in the WASP-12b discovery paper, based on spectral synthesis of four regions including the Mg b triplet at 5160-5190 Å, Na I D doublet at 5850-5950 Å, 6000-6210 Å, and Hα at 6520-6600 Å, following the procedure of Valenti & Fischer (2005).

Coupling their atmospheric modeling and retreival methods to published secondary eclipse photometry and spectroscopy spanning 0.9 μm to 8 μm, Madhusudhan et al. (2011) and Madhusudhan (2012) suggest that WASP-12b's atmosphere has a C/O ratio$\geq$1. Their best fit describes an atmosphere abundant in CO, depleted in H_2O, and enhanced in CH_4, each by greater than

two orders of magnitude compared to the authors' solar-abundance, chemical-equilibrium models. However, this high C/O_{planet} ratio for WASP-12b's atmosphere is ruled out at the $>3\sigma$ level with new observations at 2.315 μm and reanalysis of previous observations accounting for the recently detected close M-dwarf stellar companion (Bergfors et al. 2011; Crossfield et al. 2012). Including the dilution of the reported transit and eclipse depths due to the M-dwarf, the dayside spectrum of WASP-12b is best explained by a featureless 3000 K blackbody (Crossfield et al. 2012). Subsequent data (Sing et al. 2013) do not detect metal hydrides MgH, CrH, and TiH or any Ti-bearing molecules, which were previously suggested as indicative of high-C/O ratio scenarios (Madhusudhan 2012; Swain et al. 2013).

A C/O<1 composition for WASP-12b is also consistent with the study of Line et al. (2013), who use a systematic temperature and abundance retrieval analysis, combining differential evolution MCMC with an optimal-estimation-based prior, to rule out strong temperature inversion in WASP-12b's atmosphere and thus the presence of TiO causing such an inversion. Accounting for the M dwarf companion, these authors determine a best-fit C/O ratio for WASP-12b of 0.59 (χ^2_{best}/N=2.45, with a 68% confidence interval of 0.54-0.95), suggesting that a high C/O ratio is not the explanation for WASP-12b's lack of atmospheric temperature inversion. If WASP-12b's C/O ratio really is super-solar and significantly different than its host star (0.48±0.08), this suggests that some other mechanism influenced the composition of the exoplanet during its formation/evolution. Öberg et al. (2011) note that the high C/O and substellar C/H reported by Madhusudhan et al. (2011) are only consistent with an atmosphere formed predominantly from gas accretion outside the water snowline. With our updated metallicity measurement, C/H in WASP-12 decreases to $\sim 5\times10^{-4}$, exactly in the middle of the C/H distribution spanned for the planet in Madhusudhan et al. (2011)'s best-fitting (χ^2 <7) models. Thus, by these models, the planet's C/H is just as likely to be substellar as super-stellar. More data, particularly around 3 μm (see Line et al. 2013, Figure 1), can help further constrain WASP-12b's C/O ratio and enable a more meaningful comparison between planet and host star. We note that the very recent HST/WFC3 transit spectra of WASP-12b from 1.1-1.7 μm reported by Mandell et al. (2013) are fit equally well by oxygen- and carbon-rich models of Madhusudhan et al. (2012).

4.3.2. XO-1

The hot Jupiter XO-1b's (McCullough et al. 2006) four *Spitzer/IRAC* photometric secondary eclipse observations have been explained with a solar-composition, thermally-inverted model (Machalek et al. 2008). However, it is also possible to fit the observations with a non-inverted (Tinetti et al. 2010), potentially carbon-rich atmosphere model (Madhusudhan 2012), which may include disequilibrium chemistry like photochemistry and/or transport-induced quenching (Moses et al. 2013). As the favored C/O≥1 models are heavily dependent on the 5.8 μm photometric point, new observations are necessary to confirm the carbon-rich nature of XO-1b's atmosphere. Here we find in the XO-1 host star [Fe/H] = -0.11±0.06, with [C/H] = -0.19±0.04 and [O/H] = -0.09±0.05, resulting

in C/O = 0.43±0.07.

4.3.3. TrES-2 and TrES-3

TrES-2b and TrES-3b were among the first transiting hot Jupiter exoplanets discovered (O'Donovan et al. 2006; O'Donovan et al. 2007). Both fall under the highly-irradiation "pM" class predicted to have temperature inversions in their upper atmospheres (Fortney et al. 2008). Secondary eclipses of TrES-2b and TrES-3b were observed with the CFHT Wide-field Infrared Camera 2.15 μm filter, (Croll et al. 2010a; 2010b), in *Spitzer*/IRAC's four near-IR bands (O'Donovan et al. 2010; Fressin et al. 2010, respectively). Radiative transfer analyese of Line et al. (2014) use the CFHT and *Spitzer* data indicate a range of temperature-pressure profiles are too cool for TiO and VO to be in the gas phase, which suggests that these species do not cause thermal inversions. Line et al. (2014) find that the data provide minimal constraints on the abundances of H_2O, CO_2, CO, and CH_4, and thus TrES-2b's atmospheric C/O ratio. Their best fit (χ^2_{best}/N=0.60) is 0.20, but their 68% confidence interval spans 0.021-8.25. Interestingly, the C/O ratio of TrES-2 that we derive, 0.41±0.05, has the lowest error in our sample and also the second-lowest C/O ratio value in our sample. Hence, if TrES-2b accreted much of its gas from a reservoir similar in composition to its host star, and its atmosphere remained mostly isolated from its interior, it may also have a sub-solar atmospheric C/O ratio.

For TrES-3b, radiative transfer analyses of the infrared photometry indicate that H_2O is well determined with an abundance near 10^{-4}, and CH_4 has an upper limit of $\sim10^{-6}$ (Line et al. 2014). CO_2 shows a weak upper limit $\sim10^{-4}$, derived from the 2.1 μm CO_2 band wings within the K band measurement, while CO is unconstrained due to the large uncertainty in the *Spitzer* 4.5 μm data point, combined with the fact that no other molecular absorption features of CO are probed by the current data (Line et al. 2014). Line et al. (2014) infer that C/O>1 in TrES-3b due to the relatively high-confidence limit on H_2O and the small upper limit on CH_4. However, the data provide no constraints on the CO abundance, which is expected to be the major carbon carrier in an atmosphere as hot as TrES-3b. Their best fit (χ^2_{best}/N=0.067) C/O ratio for TrES-3b is 0.22, with a 68% confidence interval of 0-0.97. The very recently published HST/WFC3 secondary eclipse observations of TrES-3b are poorly fit with a solar-composition model ($\chi^2/N = 3.04$), whereas the WFC3 data plus the existing *Spitzer* photometry are more consistent ($\chi^2/N = 0.75$) with an atmosphere model depleted in CO_2 and H_2O by a factor of 10 relative to a solar-composition model (Ranjan et al. 2014).

TrES-3's C/O ratio derived here, 0.29±0.09, also has a small error and is the lowest C/O ratio in the hot Jupiter host stars studied here. The large span in the planet's C/O ratio found by Line et al. (2014) is still too large to draw meaningful conclusions about the formation location and/or growth history of TrES-3b. However, if the degeneracy between CO and CO_2 absorption in the *Spitzer* 4.5 μm data point is broken by, for instance, observations of the 2.6 μm or 15 μm CO_2 bending band or the 5 μm CO fundamental band by SOFIA/FLITECAM (McLean et al. 2006)

or SOFIA/FORCAST (Adams et al. 2010), both the CO and CO_2 contributions could be better estimated and lead to a tighter C/O ratio constraint for TrES-3b. This system is intriguing and important for further investigation due to both our firmly sub-solar C/O ratio and the relatively metal-poor nature of the host star ([Fe/H]=-0.21±0.08, the lowest in our sample), which distinguishes TrES-3 from most other hot Jupiter hosts.

4.3.4. HD 149026

Observational constraints and extensive theoretical modeling indicate that the exoplanet HD 149026b has between 45-110 $M_\oplus$ of heavy elements in its core and surrounding envelope (Sato et al. 2005; Fortney et al. 2006; Ikoma et al. 2006; Broeg & Wuchterl 2007) , making the core of HD 149026b at least twice as massive as Saturn's, even though its radius is ∼0.86 R_{Saturn} (Triaud et al. 2010) and its mass is ∼1.2 M_{Saturn} (Sato et al. 2005). The massive core of HD 149026b challenges formation by traditional core accretion theory, and many modified formation scenarios have been suggested, including collision with an outer additional giant planet (Sato et al. 2005; Ikoma et al. 2006), accretion of planetesimals or smaller (super-Earth-sized) planets (Ikoma et al. 2006; Broeg & Wuchterl 2007; Anderson & Adams 2012), or core accretion in a disk with ×2 the heavy element mass in the solar nebula (Dodson-Robinson & Bodenheimer 2009). This latter explanation stems from the metal-rich nature of the star – more massive/metal-rich disks form planets more readily (Ida & Lin 2004ab) and metal-rich planets tend to be associated with metal-rich stars (Guillot et al. 2006; Burrows et al. 2007a; Miller & Fortney 2011). Here we find [Fe/H]=0.26±0.09 for HD 149026, which is not as high as previous studies ([Fe/H]=0.36±0.05; Sato et al. 2005), but still suggests that, overall, the initial metal abundance in the molecular cloud/disk was enhanced above solar. We measure [C/H]=0.26±0.08 and [O/H]=0.25±0.04, both enhanced above solar, resulting in a C/O ratio of 0.55±0.08, consistent with solar.

Stevenson et al. (2012) find that the *Spitzer* secondary eclipse observations of HD 149026b (at 3.6, 4.5, 5.8, 8.0, and 16 μm) can be fit using models with an atmosphere in chemical equilibrium and lacking a temperature inversion, with large amounts of CO and CO_2, and a metallicity ×30 solar (Fortney et al. 2006). The retrieval results of Line et al. (2013) also indicate the atmosphere of HD 149026b has more CO and CO_2 than CH_4, which makes sense given the planet's high temperature (∼1700 K) that favors formation of CO over CH_4 at solar abundances. There is also a peak in the Line et al. modeled composition probability distribution of the H_2O mixing ratio near $\sim 10^{-5}$. Given this H_2O abundance, and the low abundance of CH_4, the C/O ratio of HD 149026b is likely <1, but is remains poorly constrained (0.55, with a χ^2_{best}/N=0.23 fit and a 68% confidence interval of 0.45-1.0; Line et al. 2013). A better estimate of HD 149026b's C/O ratio as compared to the C/O ratio of its host star (0.55±0.08) may shed light on the planet's history and the origin of its massive core. This heavy-cored hot Jupiter system, with the host star carbon and oxygen abundances presented here, is a valuable test-bed for studying how massive planets form.

4.3.5. XO-2

The hot Jupiter XO-2b has a host star, XO-2N, with a binary companion, XO-2S, located ∼4600 AU away and not known to host a hot Jupiter-type planet (Burke et al. 2007). The stars are of similar stellar type, meaning that the non-hosting companion can be used to check for effects of planet formation on the host star, e.g., stellar atmospheric pollution. XO-2b has been observed with with HST and *Spitzer* (Machalek et al. 2009; Crouzet et al. 2012) as well as from the ground (Sing et al. 2012 & 2011; Griffith et al. 2014). Griffith et al. (2014) find, with a comprehensive analysis of all existing data, that the water abundance that best matches most of the data is consistent with an atmosphere that has the same metallicity and C/O ratio as the host star in photochemical equilibrium. However there are outlying observations, so additional measurements and needed to understand the cause for the outliers and to investigate the carbon abundance in XO-2b.

Teske et al. (2013b) derived the carbon and oxygen abundances of both binary components, and found [C/H]= +0.26±0.11 in XO-2S versus +0.42±0.12 in XO-2N, and [O/H]= +0.18±0.15 in XO-2S versus +0.34±0.16 in XO-2N. The stars are enhanced above solar in C and O, with XO-2N being slighly more carbon- and oxygen-rich. Their relative enhancements result in both having C/O=0.65±0.20. (Note that this value is slightly larger than that reported in Teske et al. 2013b because the $\log N(\mathrm{O})_{\odot}$ in this work is 8.66 versus 8.69 in Teske et al. 2013b.) Both XO-2N and XO-2S fall exactly on our linear trends with [Fe/H] discussed in §4.1 ($[\mathrm{Fe/H}]_{XO-2N}$=0.39±0.14, $[\mathrm{Fe/H}]_{XO-2N}$=0.28±0.14). The elevated-above-solar [C/H] and [O/H] values in the two stars are strong evidence that their parent molecular cloud was elevated in both carbon and oxygen. Given that their C/O ratios are identical, the key to understanding why XO-2N has a planet and XO-2S does not may lie in the exoplanet composition.

4.3.6. CoRoT-2

Of the planets around the host stars in our sample, CoRoT-2b is perhaps the most puzzling in terms of its atmospheric structure. Traditional solar composition, equilibrium chemistry models are unable to reproduce the unusual flux ratios from the three *Spitzer* channel observations (it is missing 5.8 μm) of this very massive hot Jupiter (Alonso et al. 2010; Gillon et al. 2010; Deming et al. 2011; Guillot & Havel 2011). Despite its large mass, the planet has one of the greatest radius anomalies – slower-contraction evolution models that explain the radius anomalies of other inflated planets cannot justify this case (Guillot & Havel 2011). Furthermore, the host star is young (formed within 30-40 million years; Guillot & Havel 2011), chromospherically active and the system has been suggested to be undergoing magnetic star-planet interactions due to the observed stellar spot oscillation period that is ∼10× the synodic period of the planet as seen by the rotating active longitudes (Lanza et al. 2009).

CoRoT-2b's emission data are difficult to interpret, largely because of the anomalously high 4.5/8.0 μm flux ratio. Excess CO mass loss has been suggested to enhance the 4.5 μm flux, as

has some unknown absorber acting only below ~ 5 μm (Deming et al. 2011; Guillot & Havel 2011). Alternatively the low 8 μm flux may be caused by a high C/O ratio through absorption of CH_4, HCN, and C_2H_2 absorption (Madhusudhan 2012). In addition, the lack of a 5.8 μm measurement leads to a poor constraint on the H_2O abundance, which strongly dictates the resulting C/O ratio. Wilkins et al. (2014) find that no single atmospheric model is able to reproduce of all the available CoRoT-2b data, including their new 1.1.7 μm HST/WFC3 spectra, the optical eclipse observed by *CoRoT* (Alonson et al. 2009; Snellen et al. 2010) and the previously-modeled infrared photometry. More complex models with differing C/O ratios or varying opacity sources do not provide a fit more convincing that a one-component blackbody, which in itself still misses the ground-*Spitzer* eclipse amplitudes by $\sim 1.8\sigma$ (Wilkins et al. 2014).

Disequilibrium chemistry can significantly affect CoRoT-2b's atmospheric composition. For instance, for a high C/O ratio, H_2O is predicted to be enhanced above 10^{-2} bar by $\sim$four orders of magnitude due to both transport-induced quenching and CO photochemistry in the upper atmosphere (Moses et al. 2013). HCN and other C_xH_x compounds may also result from the reaction of the leftover C with N or H_2 (Moses et al. 2013). Disequilibrium chemistry models with 0.5×solar metallicity, moderate mixing, and C/O=1.1 yield a significantly better match to the four CoRoT-2b infrared secondary eclipse observations, providing a χ^2/N=1.3, versus the solar-composition models, which provide a χ^2/N=7.2 (Moses et al. 2013).

The host star C/O ratio derived here, 0.47±0.09, is equal to $C/O_\odot$ within error, as is the overall metallicity of the host star, [Fe/H]=0.06±0.08. We note that the [C/H] value measured here for CoRoT-2 is based on only 2 carbon lines (5380 Å and 7113 Å), and the [O/H] value is based on only the O I triplet at $\sim$7775 Å; the other potential C and O lines were too weak to be reliably measured in our data. In addition, while the O I triplet NLTE corrections are nominally valid in this case because the $T_{\rm eff}$ of CoRoT-2 is $\geq$5400, implementing these corrections results in an [O/H] that is larger than the LTE case, the opposite direction of the corrections at near solar temperatures. However,$[O/H]_{\rm LTE}$=0.02, the same as $[O/H]_{\rm NLTE}$=0.06 within error (0.07 dex); if we adopt the $[O/H]_{\rm LTE}$ value, CoRoT-2's C/O ratio increases by only 0.05 dex, also within error.

CoRoT-2b's C/O ratio, while still uncertain, could plausibly be >1. Several different scenarios could account for $C/O_{\rm planet} > C/O_{\rm star}$. CoRoT-2b could have accreted carbon-rich very hot gas from the inner disk regions ($\lesssim$0.1 AU). Alternatively, the planet could have accreted the majority of its gas from beyond the H_2O snow line (causing it to be oxygen-depleted), or accreted solid material depleted in oxygen (e.g., from a "tar line" inward of the snow line; Lodders 2004). Interestingly, to explain CoRoT-2b's inflated size and large mass, Guillot & Havel (2010) propose that the CoRoT-2 system previously included multiple giant planets that collided within the last $\sim$20 million years to create the currently-observed CoRoT-2b. This scenario could result in a planet that differs significantly in composition from the original states of the impactors, potentially erasing the signatures of where/from what material in the disk the planet formed. CoRoT-2b is another candidate for which additional SOFIA observations at near- (2.6 μm, 6 μm) and mid-infrared (>20 μm) wavelengths can help better constrain the exoplanet C/O ratio and thus its formation history.

4.3.7. HD 189733

The hot Jupiter HD 189733b is one of the best-studied to date, with data spanning ∼0.3-24 μm (Barnes et al. 2007; Grillmair et al. 2007; 2008; Tinetti et al. 2007; Knutson et al. 2007; 2009; 2012; Redfield et al. 2008; Charbonneau et al. 2008; Beaulieu et al. 2008; Pont et al. 2008; Désert et al. 2009; Swain et al. 2008 & 2009a; Sing et al. 2009 & 2011; Agol et al. 2010; Gibson et al. 2012; Evans et al. 2013; Birkby et al. 2013). The first complete atmospheric study via statistical analysis with a systematic, wide parameter grid search (Madhusudhan & Seager 2009) analyzed separately spectroscopic data from 5-14 μm (Grillmair et al. 2008), photometric data at 3.6, 4.5, 5.8, 8, 16, and 24 μm (Charbonneau et al. 2008), and spectrophotometric data from 1.65-2.4 μm (Swain et al. 2009a). Madhusudhan & Seager (2009) place constraints at the ξ^2=2 level (where ξ^2 is a proxy for the reduced χ^2 using the # of data points as N) on HD 189733b's atmospheric mixing ratios of H_2O, CH_4, and CO_2 using the spectrophotometric data, as it includes features of all of these molecules as well as CO. Their resulting C/O ratio range for HD 189733b is between 0.5 and 1.

Subsequent analysis of all of the available infrared secondary eclipse measurements with the Bayesian optimal estimation retrieval scheme NEMESIS (Irwin et al. 2008) placed constraints on molecular abundances ratios of HD 189733b's atmosphere, resulting in a best-estimate C/O ratio between 0.45 and 1 for ξ^2 <0.5 and between 0.15 and 1 for ξ^2 <2 (Lee et al. 2012). However, these authors caution that the current secondary eclipse data are only able to constrain the thermal structure of HD 189733b at some pressure levels, and the mixing ratios of H_2O and CO_2 with large uncertainties ranging between 9-500×10^{-5} and 3-150×10^{-5} for ξ^2 <0.5, respectively, due to the model degeneracies. The most significant degeneracy they find is between temperature and H_2O abundance at 300 mbar pressure.

The H_2O abundance has the biggest influence on the overall shape of a hot Jupiter spectrum in thermochemical equilibrium. Moses et al. (2013) focuses on the H_2O mixing ratio constraint of ∼1×10^{-4} from Madhusudhan & Seager (2009) in their exploration of disequilibrium chemistry using the combined data sets mentioned above. In both equilibrium and disequilibrum scenarios, for their nominal temperature profile and at solar metallicity, a very narrow range of C/O ratios around 0.88 provides the H_2O abundance constraint and a good fit to the observations. The recent retrieval analysis of Line et al. (2013), using the same wavelength coverage of data, also finds a best-fit C/O ratio of 0.85 (χ^2_{best}/N=2.27 fit, with a 68% confidence interval of 0.47-0.90).

A carbon-enhanced atmosphere for HD 189733b is thus theoretically plausible and consistent with observations. Interestingly, we find the host star has C/O=0.90±0.15, matching well the best-fit C/O ratios derived for the planet's atmosphere. HD 189733 is the only star within this sample to have C/O>0.8; its C/O ratio spans 0.75-1.05 within 1σ errors. Three additional stars in our sample have have C/O>0.8 within 1σ errors.

The derived $T_{\rm eff}$ of HD 189733 is ≤5400 K, therefore the triplet $[O/H]_{\rm NLTE\,avg}$ (0.125) is not included in the final average [O/H] reported here. Instead, the triplet $[O/H]_{\rm LTE}$ (0.01±0.14) and $[O/H]_{6300}$ (−0.02±0.14) values are averaged. For stars as cool as HD 189733 there is evidence from

studies of [O/H] in several open clusters that the canonical NLTE corrections are not appropriate – $[O/H]_{LTE}$ increases in lower-temperature stars in the same cluster, the opposite of what is predicted (Schuler et al. 2006). If $[O/H]_{NLTE\,avg}$ (0.125) is included in the average, the C/O ratio of HD 189733 is reduced to 0.82, and if $[O/H]_{NLTE\,avg}$ replaces $[O/H]_{LTE}$, the C/O ratio of HD 189733 is reduced to 0.79. The C/O ratio is reduced to 0.69 if $[O/H]_{NLTE\,avg}$ is the sole oxygen abundance indicator. Alternatively, one may apply an empirical correction to $[O/H]_{LTE}$ based on the temperature of HD 189733 and the observed cluster $[O/H]_{LTE}$ anomaly (Schuler et al. 2006), which amounts to ∼0.14 dex. This increases the resulting C/O ratio to 1.20.

HD 189733's [C/H] is an outlier as compared to the rest of our sample, while its [O/H] is more consistent with the rest of the sample (Figure 4). Both measurements have some of the largest abundance errors of all the targets in our sample. Our reported [C/H]=0.22±0.13 for HD 189733 is in fact based on only one carbon line, 5380 Å, from the Keck/HIRES data, though we were able to measure two lines (5380 and 7111 Å) in the Subaru/HDS data, resulting in [C/H]=0.24±0.15. Including the 7113 Å C I line measurement from the Keck/HIRES data or the Subaru/HDS data increases the [C/H] from 0.22/0.24 to 0.34/0.33, and the reported C/O ratio to 1.16. Thus is appears that the C/O ratio of HD 189733 could be as low as∼0.75, but is very likely $\gtrsim$0.80, as we report here.

In order to match the desired H_2O mixing ratio, the C/O ratio of the exoplanet HD 189733b's atmosphere must shift to higher values when its metallicity is increased – with an increase of 3×solar in metallicity the C/O ratio reaches ∼0.96, compared to our derived C/O of 0.90±0.15. Alternatively, if the metallicity is sub-solar, the required C/O ratio decreases (Moses et al. 2013). Unfortunately with present data the metallicity of HD 189733b's atmosphere is unknown. We find [Fe/H]=0.01±0.15 in the host star, providing at least a first-order constraint on the planetary atmospheric metallicity, but not a better constraint on its C/O ratio. However, we note that based on Moses et al. (2013)'s models, a change in the exoplanet's C/O ratio from 0.5 (solar) to 0.88 results in a change in the CH_4 abundance by ∼an order of magnitude, which should produce observable spectral signatures in the exoplanet's atmosphere.

4.3.8. Future of Direct Planet-Star Comparisons

The fact that HD 189733b is one of the most-studied hot Jupiters and yet still has a C/O ratio that can be anywhere from ∼0.5-1 indicates the difficulty and uncertainty in deriving exoplanet abundance ratios. Current limitations due larger to the paucity of data, which gives rise to degenerate solutions for transiting planet spectroscopy (e.g., Griffith 2013). However, as observational efforts continue to improve the quantity and quality of the measurements more precise C/O ratios will be possible. In addition, studies of transiting planets at high spectral resolution are becoming progressively refined (e.g., Snellen et al. 2010; Birkby et al. 2013; de Kok et al. 2013; Brogi et al. 2013) to the point that C/O ratio constraints are expected in the near future.

Complementary sutides of younger, hotter planets are possible with spectroscopy of directly imaged planets. One such system, HR 8799, is particularly promising as it has four directly-imaged planets of similar luminosities, masses, and radii but different orbital distances and, surprisingly, maybe even different compositions (Barman et al. 2011a; Currie et al. 2011; Galicher et al. 2011; Marley et al. 2012; Skemer et al. 2012, 2013; Konopacky et al. 2013). Recent directly-imaged, moderate-resolution (R ∼4000) spectra from ∼1.97-2.38 μm of HR 8799c show absorption of CO and H_2O but little to no CH_4 (mixing ratio $<10^{-5}$). χ^2 minimization modeling of these data finds best-fit log$N$(C) and log$N$(O) values of 8.33 and 8.51, respectively, indicating HR 8799c is depleted in both C and O with respect to solar, and resulting in a C/O ratio of $0.65^{+0.10}_{-0.05}$ (Konoapacky et al. 2013). The host star is classified as both γ Doradus and λ Bootis, making stellar abundance analysis challenging, but one previous study of the star derives C/O=0.56±0.21 (Sadakane 2006). Determining the C/O ratios of the other planetary components in this system, and other multi-planet systems, may provide constraints on how the composition of the host star affects giant planet formation as a function of planet mass and orbital radius.

5. Summary

The differences between [Fe/H] distributions in hosts versus non-hosts have been the subject of study for over a decade, and a few more recent studies suggest that refractory element distributions may differ in stars with/without planets, but differences in volatile elements have not been as thoroughly explored. Here we present a uniform stellar parameter and abundance analysis of 16 stars that host transiting hot Jupiter exoplanets. Our study also includes one binary companion that is not known to host planets. This work presents detailed measurements of transiting exoplanet host star carbon and oxygen abundances, derived using muliple indicators of oxygen abundance. The derived host star C/O ratios contribute one component to the direct comparison of stellar and exoplanetary atmospheric compositions.

We compare our results to other studies of C/O vs. [Fe/H] in exoplanet host stars, and find a similar positive slope between these two parameters. This is indicative of Galactic chemical evolution and the increasing importance of the carbon contribution from the death of low- and intermediate-mass stars at more metal-rich times in the Galaxy. A linear fit to our [C/H] versus [Fe/H] data results in a slope ∼twice that of a linear fit to our [O/H] vs. [Fe/H], with the former relation passing 0.08 dex below solar and the latter passing 0.01 above solar. We derive a linear fit of C/O=0.53[Fe/H] + 0.45 to our data, which falls 0.09 below our adopted $C/O_\odot$=0.54, but corresponds to a 0.08 dex difference in [C/O], similar to the offsets in [C/H] and [O/H] relations. These offsets likely reflect both analysis uncertainties and the real, intrinsic scatter in Galactic disk populations.

There is agreement between the average [C/H], [O/H], and C/O values found here and the results of other studies of RV-detected planet host stars, supporting previous findings (Ammler von-Eiff et al. 2009) that elemental abundance ratios do not differ significantly between transiting

and RV-planet host stars. The mean C/O ratio of the transiting exoplanet host stars in this paper is slightly lower than that found by other studies that consist of non-transiting host stars, 0.54±0.15 versus 0.71±0.07. This is more in line with recent suggestions that the prior studies overestimated C/O ratios.

Several cases in which the process of directly comparing the chemistry in specific stars to their planets is already beginning are highlighted – WASP-12, XO-1, TrES-2, TrES-3, HD 149026, XO-2, CoRoT-2, and HD 189733. We encourage follow-up observational and theoretical studies of all of the exoplanets whose host stars are included in this paper. Facilities that are currently available in space and on the ground can be used strategically to obtain estimates of C/O ratios of a large sample of transiting exoplanets, which JWST and several other upcoming space-based missions (e.g., EChO) will be able to better characterize. The more precise abundance analysis that is possible right now for host stars can help infer their exoplanets' formation histories, as well as inform future planet formation theories and models.

The authors wish to recognize and acknowledge the very significant cultural role and reverence that the summit of Mauna Kea has always had within the indigenous Hawaiian community. We are most fortunate to have the opportunity to conduct observations from this mountain. This work would not have been possible without the efforts of the daytime and nighttime support staff at the Mauna Kea Observatory and Subaru Telescope, particularly Akito Tajitsu, Rita Morris, and Jennie Berghuis. The authors also thank the anonymous referee for her/his helpful corrections and comments. The work of J. T. and C. G. is suppored by NASA's Planetary Atmospheres Program. J.T. thanks Andy Skemer for his aid in interpreting directly-imaged planet results. This research has made use of the Exoplanet Orbit Database and the Exoplanet Data Explorer at exoplanets.org.

Facilities: Subaru, Keck

REFERENCES

Agol, E., Cowan, N. B., Knutson, H. A., et al. 2010, ApJ, 721, 1861

Ali-Dib, M., Mousis, O., Pekmezci, G. S., et al. 2014, A&A, 561, A60

Ammler-von Eiff, M., Santos, N. C., Sousa S. G., Fernandes, J., Guillot, T., Israelian, G., Mayor, M., Melo, C., 2009, A&A, 507, 523

Anderson, K. R., & Adams, F. C. 2012, PASP, 124, 809

Asplund, M. 2005, ARA&A, 43, 481

Asplund, M., Grevesse, N., & Sauval, A. J. 2005, Cosmic Abundances as Records of Stellar Evolution and Nucleosynthesis, 336, 25

Asplund, M., Grevesse, N., Sauval, A. J., & Scott, P. 2009, ARA&A, 47, 481

Bailey, V., Meshkat, T., Reiter, M., et al. 2014, ApJ, 780, L4

Barman T. S., Macintosh B., Konopacky Q. M., Marois C., 2011a, ApJ, 733, 65

Barman T. S., Macintosh B., Konopacky Q. M., Marois C., 2011b, ApJ, 735, L39

Barnes, J. R., Barman, T. S., Prato, L., et al. 2007, MNRAS, 382, 473

Beaulieu, J. P., Carey, S., Ribas, I., & Tinetti, G. 2008, ApJ, 677, 1343

Beaulieu, J. P., Kipping, D. M., Batista, V., et al. 2010, MNRAS, 409, 963

Bensby, T., Feltzing, S., & Lundström, I. 2004, A&A, 415, 155

Bergfors, C., Brandner, W., Henning, T., & Daemgen, S. 2011, IAU Symposium, 276, 397

Birkby, J. L., de Kok, R. J., Brogi, M., et al. 2013, MNRAS, 436, L35

Bond, J. C., O'Brien, D. P., & Lauretta, D. S. 2010, ApJ, 715, 1050

Bond, J. C., Tinney, C. G., Butler, R. P., et al. 2006, MNRAS, 370, 163

Bond, J. C., Lauretta, D. S., Tinney, C. G., et al. 2008, ApJ, 682, 1234

Broeg C., Wuchterl G., 2007, MNRAS, 376, L62

Brogi, M., Snellen, I. A. G., de Kok, R. J., et al. 2013, ApJ, 767, 27

Brown, D. J. A., Collier Cameron, A., Díaz, R. F., et al. 2012, ApJ, 760, 139

Brugamyer, E., Dodson-Robinson, S. E., Cochran, W. D., & Sneden, C. 2011, ApJ, 738, 97

Buchhave, L. A., et al., 2012, Nature, 486, 375

Buchhave, L. A., Bakos, G. Á., Hartman, J. D., et al. 2010, ApJ, 720, 1118

Burke, C. J., et al., 2007, ApJ, 671, 2115

Burrows A., Hubeny I., Budaj J., Hubbard W. B., 2007a, ApJ, 661, 502

Caffau, E., Ludwig, H.-G., Malherbe, J.-M., et al. 2013, A&A, 554, A126

Caffau, E., Ludwig, H.-G., Steffen, M., Freytag, B., & Bonifacio, P. 2011, Sol. Phys., 268, 255

Caffau, E., Ludwig, H.-G., Bonifacio, P., et al. 2010, A&AP, 514, A92

Caffau, E., Ludwig, H.-G., Steffen, M., et al. 2008, A&A, 488, 1031

Cassan, A., et al. 2012, Nature, 481, 167

Charbonneau D., et al., 2005, ApJ, 626, 523

Charbonneau D., Knutson H. A., Barman T., Allen L. E., Mayor M., Megeath S. T., Queloz D., Udry S. , 2008, ApJ, 686, 1341

Ciesla, F. J., & Cuzzi, J. N. 2006, Icarus, 181, 178

Copperwheat, C. M., Wheatley, P. J., Southworth, J., et al. 2013, MNRAS, 434, 661

Crossfield, I. J. M., Barman, T., Hansen, B. M. S., Tanaka, I., & Kodama, T. 2012, ApJ, 760, 140

Crouzet, N., McCullough, P. R., Burke, C., & Long, D. 2012, ApJ, 761, 7

Currie T., et al., 2011, ApJ, 729, 128

Davis, S. P. & Phillips, J. G. 1963, Berkeley Analyses of Molecular Spectra, Berkeley: University of California Press

de Kok, R. J., Brogi, M., Snellen, I. A. G., et al. 2013, A&A, 554, A82

Désert, J.-M., Lecavelier des Etangs, A., Hébrard, G., Sing, D. K., Ehrenreich, D., Ferlet, R., Vidal-Madjar, A., 2009, ApJ, 699, 478

Delgado Mena, E., Israelian, G., González Hernández, J. I., Bond, J. C., Santos, N. C., Udry, S., Mayor, M., 2010, ApJ, 725, 2349

Dodson-Robinson, S. E., & Bodenheimer, P. 2009, ApJ, 695, L159

Ecuvillon, A., Israelian, G., Santos, N. C., et al. 2004, A&A, 426, 619

Ecuvillon, A., Israelian, G., Santos, N. C., Mayor, M., & Gilli, G. 2006, A&A, 449, 809

Evans, T. M., Pont, F., Sing, D. K., et al. 2013, ApJ, 772, L16

Everett, M. E., Howell, S. B., Silva, D. R., & Szkody, P. 2013, ApJ, 771, 107

Fabbian, D., Asplund, M., Barklem, P. S., Carlsson, M., & Kiselman, D. 2009, A&A, 500, 1221

Favre, C., Cleeves, L. I., Bergin, E. A., Qi, C., & Blake, G. A. 2013, ApJ, 776, L38

Fazio, G. G., Hora, J. L., Allen, L. E., et al. 2004, ApJS, 154, 10

Fischer, D. A., & Valenti, J. 2005, ApJ, 622, 1102

Fitzpatrick, M. J., & Sneden, C. 1987, BAAS, 19, 1129

Fortney J. J., Saumon D., Marley M. S., Lodders K., Freedman R. S., 2006, ApJ, 642, 495

Fortney, J. J. 2012, ApJ, 747, L27

Gaidos, E. J. 2000, Icarus, 145, 637

Gaidos, E., Fischer, D. A., Mann, A. W., & Howard, A. W. 2013, ApJ, 771, 18

Galicher R., Marois C., Macintosh B., Barman T., Konopacky Q., 2011, ApJ, 739, L41

Ghezzi, L., Cunha, K., Smith, V. V., de Araújo, F. X., Schuler, S. C., de la Reza, R., 2010, ApJ, 720, 1290

Gibson, N. P., Aigrain, S., Pont, F., et al. 2012, MNRAS, 422, 753

Gonzalez, G. 1998, A&A, 334, 221

Gonzalez, G., Laws, C., Tyagi, S., & Reddy, B. E. 2001, AJ, 121, 432

González Hernández, J. I., Israelian, G., Santos, N. C., Sousa, S., Delgado-Mena, E., Neves, V., Udry, S., 2010, ApJ, 7

González Hernández, J. I., Delgado-Mena, E., Sousa, S. G., et al. 2013, A&A, 552, A6

Gratton, R. G., Carretta, E., Eriksson, K., & Gustafsson, B. 1999, A&A, 350, 955

Griffith, C. A. 2013, arXiv:1312.3988

Griffith, C. A. et al. 2014, in prep.

Grillmair, C. J., Charbonneau, D., Burrows, A., et al. 2007, ApJ, 658, L115

Grillmair C. J., et al., 2008, Nature, 456, 767

Guillot T., Santos N. C., Pont F., Iro N., Melo C., Ribas I., 2006, A&A, 453, L21

Gustafsson, B., Edvardsson, B., Eriksson, K., et al. 2008, A&A, 486, 951

Hebb, L., Collier-Cameron, A., Loeillet, B., et al. 2009, ApJ, 693, 1920

Hibbert, A., Biemont, E., Godefroid, M., & Vaeck, N. 1991, Journal of Physics B Atomic Molecular Physics, 24, 3943

Ida, S., & Lin, D. N. C. 2004a, ApJ, 604, 388

Ida, S., & Lin, D. N. C. 2004b, ApJ, 616, 567

Ikoma M., Guillot T., Genda H., Tanigawa T., Ida S., 2006, ApJ, 650, 1150

Irwin, P. G. J., Teanby, N. A., de Kok, R., et al. 2008, J. Quant. Spec. Radiat. Transf., 109, 1136

Janson, M., Brandt, T. D., Kuzuhara, M., et al. 2013, ApJ, 778, L4

Johansson, S., Litzén, U., Lundberg, H., & Zhang, Z. 2003, ApJ, 584, L107

Johnson, T. V., Mousis, O., Lunine, J. I., & Madhusudhan, N. 2012, ApJ, 757, 192

Johnson, J. A., Aller, K. M., Howard, A. W., & Crepp, J. R. 2010, PASP, 122, 905

Kiselman, D. 1993, A&A, 275, 269

Kiselman, D. 2001, NAR, 45, 559

Knutson, H. A., Charbonneau, D., Allen, L. E., Burrows, A., & Megeath, S. T. 2008, ApJ, 673, 526

Knutson, H. A., Charbonneau, D., Allen, L. E., et al. 2007, Nature, 447, 183

Knutson, H. A., Charbonneau, D., Cowan, N. B., et al. 2009, ApJ, 690, 822

Knutson, H. A., Lewis, N., Fortney, J. J., et al. 2012, ApJ, 754, 22

Konopacky, Q. M., Barman, T. S., Macintosh, B. A., & Marois, C. 2013, Science, 339, 1398

Kupka, F., Piskunov, N., Ryabchikova, T. A., Stempels, H. C., & Weiss, W. W. 1999, A&AS, 138, 119

Kurucz, R. L. 1992, The Stellar Populations of Galaxies, 149, 225

Kurucz, R. 1993, Opacities for Stellar Atmospheres: Abundance Sampler. Kurucz CD-ROM No. 14. Cambridge, Mass.: Smithsonian Astrophysical Observatory, 1993., 14,

Kurucz, R. L. 1996, M.A.S.S., Model Atmospheres and Spectrum Synthesis, 108, 2

Lagrange A.-M., et al., 2009, A&A, 493, L21

Laws, C., & Gonzalez, G. 2001, ApJ, 553, 405

Lee, J.-M., Fletcher, L. N., & Irwin, P. G. J. 2012, MNRAS, 420, 170

Line, M. R., Knutson, H., Wolf, A. S., & Yung, Y. L. 2014, ApJ, 783, 70

Lodders, K. 2010, Principles and Perspectives in Cosmochemistry, 379

Machalek P., McCullough P. R., Burke C. J., Valenti J. A., Burrows A., Hora J. L., 2008, ApJ, 684, 1427

Machalek P., McCullough P. R., Burrows A., Burke C. J., Hora J. L., Johns-Krull C. M., 2009, ApJ, 701, 514

Madhusudhan, N., & Seager, S. 2009, ApJ, 707, 24

Madhusudhan, N., et al. 2011, Nature, 469, 64

Madhusudhan, N. 2012, ApJ, 758, 36

Mandell, A. M., Haynes, K., Sinukoff, E., et al. 2013, ApJ, 779, 128

Marley M. S., Saumon D., Cushing M., Ackerman A. S., Fortney J. J., Freedman R., 2012, ApJ, 754, 135

Marois C., Macintosh B., Barman T., Zuckerman B., Song I., Patience J., Lafrenière D., Doyon R., 2008, Sci, 322, 1348

Marois C., Zuckerman B., Konopacky Q. M., Macintosh B., Barman T., 2010, Nature, 468, 1080

Maxted, P. F. L., Aderson, D. R., Collier Cameron, A., et al. 2010, PASP, 122, 1465

McCullough P. R., et al., 2006, ApJ, 648, 1228

Meléndez, J., Asplund, M., Gustafsson, B., & Yong, D. 2009, ApJ, 704, L66

Miller, N., & Fortney, J. J. 2011, ApJ, 736, L29

Mortier, A., Santos, N. C., Sousa, S. G., et al. 2013, A&A, 558, A106

Moses J. I., et al., 2011, ApJ, 737, 15

Moses, J. I., Madhusudhan, N., Visscher, C., & Freedman, R. S. 2013, ApJ, 763, 25

Najita J. R., Carr J. S., Pontoppidan K. M., Salyk C., van Dishoeck E. F., Blake G. A., 2013, ApJ, 766, 134

Nissen, P. E. 2013, arXiv:1303.1726

Noguchi, K., et al. 2002, PASJ, 54, 855

Öberg, K. I., Murray-Clay, R., & Bergin, E. A. 2011, ApJ, 743, L16

Owen, T., Mahaffy, P., Niemann, H. B., et al. 1999, Nature, 402, 269

Piskunov, N. E., Kupka, F., Ryabchikova, T. A., Weiss, W. W., & Jeffery, C. S. 1995, A&AS, 112, 525

Petigura, E. A., & Marcy, G. W. 2011, ApJ, 735, 41

Pollack, J. B., Hubickyj, O., Bodenheimer, P., et al. 1996, Icarus, 124, 62

Pont, F., Hébrard, G., Irwin, J. M., et al. 2009, å, 502, 695

Pont, F., Knutson, H., Gilliland, R. L., Moutou, C., & Charbonneau, D. 2008, MNRAS, 385, 109

Ramírez, I., Allende Prieto, C., & Lambert, D. L. 2007, A&A, 465, 271

Ramírez, I., Meléndez, J., & Asplund, M. 2014, A&A, 561, A7

Ranjan, S., Charbonneau, D., Désert, J. M., et al. 2014, arXiv:1403.1266

Redfield, S., Endl, M., Cochran, W. D., & Koesterke, L. 2008, ApJ, 673, L87

Ryabchikova T.A., Piskunov N.E., Kupka F., Weiss W.W., 1997, Baltic Astronomy, vol. 6, 244-247

Sadakane, K. 2006, PASJ, 58, 1023

Santos, N. C., Israelian, G., & Mayor, M. 2004, A&A, 415, 1153

Santos, N. C., Sousa, S. G., Mortier, A., et al. 2013, A&A, 556, A150

Sato B., et al., 2005, ApJ, 633, 465

Schuler, S. C., Flateau, D., Cunha, K., King, J. R., Ghezzi, L., Smith, V. V., 2011a, ApJ, 732, 55

Schuler, S. C., Cunha, K., Smith, V. V., Ghezzi, L., King, J. R., Deliyannis, C. P., Boesgaard, A. M., 2011b, ApJ, 737, L32

Sing, D. K., Désert, J.-M., Lecavelier Des Etangs, A., et al. 2009, A&A, 505, 891

Sing, D. K., Désert, J.-M., Fortney, J. J., et al. 2011, A&A, 527, A73

Sing, D. K., Huitson, C. M., Lopez-Morales, M., et al. 2012, MNRAS, 426, 1663

Sing, D. K., Lecavelier des Etangs, A., Fortney, J. J., et al. 2013, MNRAS, 436, 2956

Skemer A. J., et al., 2012, ApJ, 753, 14

Skemer, A. J., Marley, M. S., Hinz, P. M., et al. 2013, arXiv:1311.2085

Sneden, C. 1973, ApJ, 184, 839

Sneden, C., & Lambert, D. L. 1982, ApJ, 259, 381

Snellen, I. A. G., de Kok, R. J., de Mooij, E. J. W., & Albrecht, S. 2010, Nature, 465, 1049

Sousa S. G., Santos N. C., Israelian G., Mayor M., Monteiro M. J. P. F. G., 2007, A&A, 469, 783

Snellen, I. A. G., de Kok, R. J., de Mooij, E. J. W., & Albrecht, S. 2010, Nature, 465, 1049

Stevenson, D. J., & Lunine, J. I. 1988, Icarus, 75, 146

Stevenson K. B., et al., 2012, ApJ, 754, 136

Storey, P. J., & Zeippen, C. J. 2000, MNRAS, 312, 813

Swain, M. R., Vasisht, G., & Tinetti, G. 2008, Nature, 452, 329

Swain, M. R., Vasisht, G., Tinetti, G., et al. 2009a, ApJ, 690, L114

Swain, M. R., Tinetti, G., Vasisht, G., et al. 2009b, ApJ, 704, 1616

Swain, M., Deroo, P., Tinetti, G., et al. 2013, Icarus, 225, 432

Takeda, Y. 2003, A&A, 402, 343

Takeda, Y., & Honda, S. 2005, PASJ, 57, 65

Teske, J. K., Schuler, S. C., Cunha, K., Smith, V. V., & Griffith, C. A. 2013a, ApJ, 768, L12

Teske, J. K., Cunha, K., Schuler, S. C., Griffith, C. A., & Smith, V. V. 2013b, ApJ, 778, 132

Tinetti, G., et al. 2007, Nature, 448, 169

Tinetti G., Deroo P., Swain M. R., Griffith C. A., Vasisht G., Brown L. R., Burke C., McCullough P., 2010, ApJ, 712, L139

Torres, G., Fischer, D. A., Sozzetti, A., Buchhave, L. A., Winn, J. N., Holman, M. J., Carter, J. A., 2012, ApJ, 757, 161

Triaud A. H. M. J., et al., 2010, A&A, 524, A25

Valenti, J. A., & Piskunov, N. 1996, A&AS, 118, 595

Vogt, S. S., Allen, S. L., Bigelow, B. C., et al. 1994, Proc. SPIE, 2198, 362

Wong, M., Lunine, J., Atreya, S., Johnson, T., Mahaffy, P., Owen, T., & Encrenaz, T. 2008, Reviews in Mineralogy and Geochemistry, 68, 219

This preprint was prepared with the AAS LaTeX macros v5.2.

Table 1. Observing Log

Star	V	Date (UT)	Exposures	T_{exp} (s)	Platform
CoRoT-2	12.57	2013 Aug 30	3	1500	Keck/HIRES
TrES-4	11.59	2013 Aug 30	2	1920, 900	Keck/HIRES
TrES-2	11.25	2013 Aug 30	1	1320	Keck/HIRES
WASP-2	11.98	2013 Aug 30	2	1440	Keck/HIRES
WASP-12	11.57	2012 Feb 10	3	1080 (2), 1800 (1)	Subaru/HDS
		2012 Feb 11	2	1800	Subaru/HDS
XO-2	11.25	2012 Feb 10	2	1800	Subaru/HDS
XO-2B	11.20	2012 Feb 11	2	2100	Subaru/HDS
XO-1	11.25	2012 Feb 10	2	1800	Subaru/HDS
TrES-3	12.40	2012 Feb 10	2	2400	Subaru/HDS
		2012 Feb 11	2	2100	Subaru/HDS
		2008 Jun 12	17	1200 (12), 600 (3), 420, 45	Keck/HIRES archive
HD 189733	7.68	2012 Feb 10	2	120	Subaru/HDS
		2006 Aug 21	3	208, 212, 226	Keck/HIRES archive
HD 149026	8.14	2012 Feb 11	1	480	Subaru/HDS
		2005 Jun 29	3	171,179,176	Keck/HIRES archive
HD 80606	9.00	2012 Feb 11	2	600	Subaru/HDS
HAT-P-7	10.48	2012 Feb 10	1	900	Subaru/HDS
		2012 Feb 11	2	1200	Subaru/HDS
		2007 Aug 24	1	600	Keck/HIRES archive
HAT-P-13	10.42	2012 Feb 11	1	1800	Subaru/HDS
HAT-P-1	10.4	2012 Aug 31	2	500, 630	Keck/HIRES
HAT-P-16	10.91	2012 Aug 31	2	1120, 1043	Keck/HIRES
WASP-32	11.26	2012 Aug 31	2	1500, 1800	Keck/HIRES
Moon		2012 Feb 10	2	1, 5	Subaru/HDS
Vesta		2006 Apr 16	3	216, 232, 241	Keck/HIRES archive

Table 2. Observing Platform Details

Platform	slit (and filter, if applicable)	R ($\frac{\lambda}{\Delta\lambda}$)	Wavelength Coverage (Å)	S/N of combined frames (at 6300 Å)	Seeing Range
Subaru/HDS	0."6	60,000	∼4450-5660; 5860-7100*	∼170-230	0."84-1."12; 0."96-1."24^{+}
Keck/HIRES	0."86 (C1 decker) kv370+clear filters	48,000	∼3360-8100	∼125-150	∼0.4-0.6"; ∼0.6-0.8"$^{++}$
Keck/HIRES archive					
HAT-P-7	same	same	same	∼190	
HD 189733	same	same	same	∼250	
HD 149026	same	same	same	∼290	
Vesta	same	same	same	∼315	
TrES-3	0."57, kv389 filter	72,000	4240-8690	∼300	

*Wavelength coverage across two separate CCDs.

$^{+}$Seeing from Feb. 10; Feb. 11.

$^{++}$Seeing from Aug. 31, 2012; Aug. 30, 2013

Note. — We note that the TrES-3 Keck/HIRES archive observations used a different filter and narrower slit, and thus had slightly different wavelength coverage and higher resolution, but this did not affect our ability to measure the necessary elemental absorption lines.

Table 3. Derived Stellar Parameters

Star	T_{eff} K	σ K	log g	σ	ξ km s^{-1}	σ km s^{-1}	[Fe I/H]	N	σ_μ	[Fe II/H]	N	σ_μ
CoRot-2	5616	47	4.52	0.14	1.59	0.09	0.063	48	0.007	0.064	7	0.017
TrES-4	6333	44	4.04	0.17	1.74	0.09	0.320	49	0.005	0.322	9	0.025
TrES-2	5823	33	4.45	0.10	1.27	0.07	-0.016	51	0.004	-0.016	9	0.005
WASP-2	5228	60	4.49	0.21	1.07	0.10	0.092	52	0.008	0.091	9	0.021
WASP-12	6166	41	4.05	0.16	1.95	0.13	0.062	40	0.006	0.062	10	0.020
XO-2N	5343	78	4.49	0.25	1.22	0.09	0.386	49	0.011	0.389	8	0.020
XO-2S	5547	59	4.22	0.24	1.24	0.07	0.291	50	0.010	0.295	10	0.048
XO-1	5695	26	4.42	0.12	1.39	0.06	−0.109	36	0.004	−0.110	9	0.008
TrES-3	5534	42	4.56	0.14	1.20	0.10	−0.209	33	0.007	−0.206	8	0.021
HD 189733	5116	76	4.64	0.25	1.27	0.16	0.012	43	0.012	0.011	9	0.041
HD 149026	6093	48	4.30	0.21	1.71	0.09	0.265	51	0.007	0.264	9	0.024
HD 80606	5551	47	4.14	0.17	1.29	0.06	0.274	41	0.008	0.275	8	0.046
HAT-P-7	6474	71	4.33	0.29	2.72	0.37	0.140	40	0.008	0.139	10	0.033
HAT-P-13	5775	57	4.13	0.17	1.44	0.07	0.442	51	0.009	0.445	10	0.035
HAT-P-1	6045	44	4.52	0.12	1.51	0.11	0.172	53	0.006	0.174	8	0.012
HAT-P-16	6236	58	4.49	0.19	1.58	0.15	0.174	54	0.007	0.172	9	0.015
WASP-32	6042	42	4.34	0.20	1.80	0.15	−0.066	53	0.006	−0.069	9	0.023

Table 4. Lines Measured, Equivalent Widths, and Abundances

Ion	λ	χ	log gf	EW$_\odot$	log$N_\odot$	WASP-12			HD 149026			HAT-P-1	
	(Å)	(eV)	(dex)	(mÅ)		EW (mÅ)	log N		EW (mÅ)	log N		EW (mÅ)	log N
C I	5052.17	7.68	-1.304	33.9[a], 33.7[b]	8.46[a], 8.45[b]	62.4[a]	8.58[a]	···	···	···	···	43.9[b]	8.51[b]
	5380.34	7.68	-1.615	19.4[a], 20.7[b]	8.44[a], 8.48[b]	41.1[a]	8.57[a]	···	44.5[b]	8.76[b]	···	29.3[b]	8.56[b]
	6587.61	8.54	-1.021	12.9[a], 15.5[b]	8.38[a], 8.48[b]	27.0[a]	8.4[a]	···	36.4[b]	8.75[b]	···	20.2[b]	8.46[b]
	7111.47	8.64	-1.074	9.8[a], 12.2[b]	8.38[a], 8.50[b]	21.0[a]	8.42[a]	···	26.6[b]	8.69[b]	···	16.3[b]	8.49[b]
	7113.18	8.65	-0.762	22.8[a], 20.9[b]	8.55[a], 8.50[b]	···	···	···	47.4[b]	8.79[b]	···	29.2[b]	8.53[b]
[OI]*	6300.30	0.00	-9.717	5.4[a], 5.6[b]	8.68[a], 8.67[b]	7.0[a]	8.82[a]	···	8.2[b]	8.95[b]	···	4.6[b]	8.62[b]
O I	7771.94	9.15	0.37	69.6[b]	8.83[b]	···	···	···	119.8[b]	9.17[b]	···	89.7[b]	8.88[b]
O I	7774.17	9.15	0.22	62.6[b]	8.86[b]	···	···	···	108.6[b]	9.18[b]	···	···	···
O I	7775.39	9.15	0.00	46.8[b]	8.81[b]	···	···	···	82.0[b]	9.05[b]		61.1[b]	8.83[b]

[a]Measured in the Subaru/HDS data.

[b]Measured in the Keck/HIRES data.

*For [O I], the log N values represent those derived from synthesis fitting, as these are the values we use in calculating the final [O/H] for each object. The reported EWs refer to the total EW of the 6300.3 Å blend.

Note. — The full version of this table including all lines and targets is available online.

Table 5. Oxygen Abundances Derived from Different Indicators

Star	[O/H] [O I] 6300 Å	[O/H] triplet LTE	[O/H] triplet NLTE, Takeda	[O/H] triplet NLTE, Ramírez	[O/H] triplet NLTE, Fabbian
CoRoT-2*	···	0.02±0.07	0.07	0.06	0.07
TrES-4*	0.22±0.09	0.31±0.07	0.15	0.21	0.08
TrES-2*	-0.02±0.05	0.00±0.05	0.02	0.01	-0.01
WASP-2*	-0.03±0.10	-0.01±0.10	0.08	0.06	0.09
WASP-12	0.14±0.06	···	···	···	···
XO-2N	0.34±0.16	···	···	···	···
XO-2S	0.18±0.15	···	···	···	···
XO-1	−0.09±0.05	···	···	···	···
TrES-3*	−0.04±0.06	···	···	···	
HD 189733*	−0.02±0.14	0.01±0.14	0.12	0.11	0.14
HD 149026*	0.28±0.03	0.30±0.07	0.21	0.26	0.20
HD 80606	0.20±0.08	···	···	···	···
HAT-P-7*	···	0.22±0.10	0.06	0.11	0.02
HAT-P-13	0.19±0.08	···	···	···	···
HAT-P-1*	−0.05±0.06	0.07±0.06	0.07	0.07	0.02
HAT-P-16*	−0.08±0.10	0.04±0.06	0.03	−0.01	−0.10
WASP-32*	−0.08±0.09	0.08±0.08	0.03	0.00	−0.01

*Measurements from Keck/HIRES data.

Table 6. Elemental Abundances and Ratios

Star	[Fe/H]	[C/H]	$[O/H]_{avg}$	[Ni/H]	C/O_{avg}
CoRoT-2	0.06±0.08*	0.01±0.06*	0.06±0.07*	-0.08±0.03*	0.47±0.09*
TrES-4	0.32±0.09*	0.11±0.06*	0.18±0.06*	0.29±0.02*	0.46±0.08*
TrES-2	-0.02±0.05*	-0.12±0.04*	-0.01±0.04*	-0.08±0.02*	0.41±0.05 *
WASP-2	0.09±0.12*	-0.01±0.09*	-0.02±0.07*	0.11±0.03*	0.55±0.11*
WASP-12	0.06±0.08	0.09±0.06	0.14±0.06	0.00±0.04	0.48±0.08
XO-2N	0.39±0.14	0.42±0.12	0.34±0.16	0.44±0.04	0.65±0.20
XO-2S	0.28±0.14	0.26±0.11	0.18±0.15	0.38±0.04	0.65±0.19
XO-1	−0.11±0.06	−0.19±0.04	−0.09±0.05	−0.11±0.02	0.43±0.07
TrES-3	−0.21±0.08	−0.31±0.06*	−0.04±0.06*	−0.25±0.04	0.29±0.09*
HD 189733	0.01±0.15	0.22±0.11*	-0.01±0.10*	0.00±0.05	0.90±0.15*
HD 149026	0.26±0.09	0.26±0.08*	0.25±0.04*	0.31±0.03	0.55±0.08*
HD 80606	0.28±0.10	0.29±0.08	0.20±0.08	0.30±0.03	0.66±0.12
HAT-P-7	0.14±0.14	−0.04 ±0.10*	0.07±0.10*	0.12±0.05	0.42±0.14*
HAT-P-13	0.44±0.09	0.34±0.08	0.19±0.08	0.53±0.04	0.76±0.11
HAT-P-1	0.17±0.06*	0.03±0.05*	0.00±0.04*	0.17±0.03*	0.58±0.06*
HAT-P-16	0.17±0.09*	−0.02±0.06*	−0.05±0.06*	0.13±0.04*	0.58±0.08*
WASP-32	−0.07±0.09*	−0.09±0.07*	−0.04±0.06*	−0.13±0.03*	0.47±0.09*

Note. — $C/O=10^{logN(C)}/10^{logN(O)}$, with $\log N(C)$=derived [C/H]+$\log N_{\odot}(C)$ and $\log N(O)$=derived [O/H]+$\log N_{\odot}(O)$, where $\log N_{\odot}(O)$=8.66 and $\log N_{\odot}(C)$=8.39 (solar values from Asplund et al. 2005). The errors on the C/O ratio are represented by the quadratic sum of the errors in [C/H] and [O/H].

*Measurements include Keck/HIRES data.

Table 7. Abundance Sensitivities

Species	WASP-12			HAT-P-1		
	ΔT_{eff} (±150 K)	$\Delta \log g$ (±0.25 dex)	$\Delta\xi$ (±0.30 km s^{-1})	ΔT_{eff} (±150 K)	$\Delta \log g$ (±0.25 dex)	$\Delta\xi$ (±0.30 km s^{-1})
Fe I	±0.10	±0.005	±0.03	±0.09	±0.005	±0.03
Fe II	±0.02	±0.10	±0.08	±0.05	±0.10	±0.07
C I	±0.08	±0.08	±0.01	±0.10	±0.08	±0.005
[OI]*	±0.06	±0.09	±0.01	±0.11	±0.12	±0.00
Ni I	±0.11	±0.02	±0.03	±0.10	±0.005	±0.04
O I triplet (LTE)	···	···	···	±0.13	±0.07	±0.03

*For [O I], the log N values represent those derived from synthesis fitting, as these are the values we use in calculating the final [O/H] for each object.

Table 8. Comparison of Average C & O Measurements to Previous Work

Source	$\overline{[C/H]}_{\rm hosts}$	$\overline{[C/H]}_{\rm non-hosts}$	$\overline{[O/H]}_{\rm hosts}$	$\overline{[O/H]}_{\rm non-hosts}$	$\overline{C/O}_{\rm hosts}$	$\overline{C/O}_{\rm non-hosts}$
Ecuvillon et al. (2004) or (2006)	0.14 ± 0.10	−0.03 ±0.14	0.12 ± 0.11	0.07 ± 0.15	···	···
Bond et al. (2006) or (2008)	0.17 ± 0.11	0.01 ± 0.17	0.00 ± 0.17	−0.06 ±0.15	0.67 ± 0.23	0.67 ± 0.23
Delgado Mena et al. (2010)	0.10 ± 0.16	−0.06 ± 0.18	0.05 ± 0.17	−0.08 ± 0.17	0.76 ± 0.20	0.71 ± 0.18
Petigura & Marcy (2011)	0.17 ± 0.14	0.08 ± 0.17	0.11 ± 0.12	0.05 ± 0.14	0.76 ± 0.22	0.70 ± 0.22
Nissen (2013)	0.11 ± 0.15	···	0.08 ± 0.10	···	0.63 ± 0.12	···
this work (*only transiting planets*)	0.06±0.20	···	0.07±0.13	···	0.54±0.15	···

Note. — Listed are the means and standard deviations in exoplanet hosts stars and "non-host" stars, for each elemental abundance ratio, given as (mean ± standard deviation). Note that the number of objects in each source's sample is not equal, and that different sources use different solar log$N$(C) and log$N$(O) values.

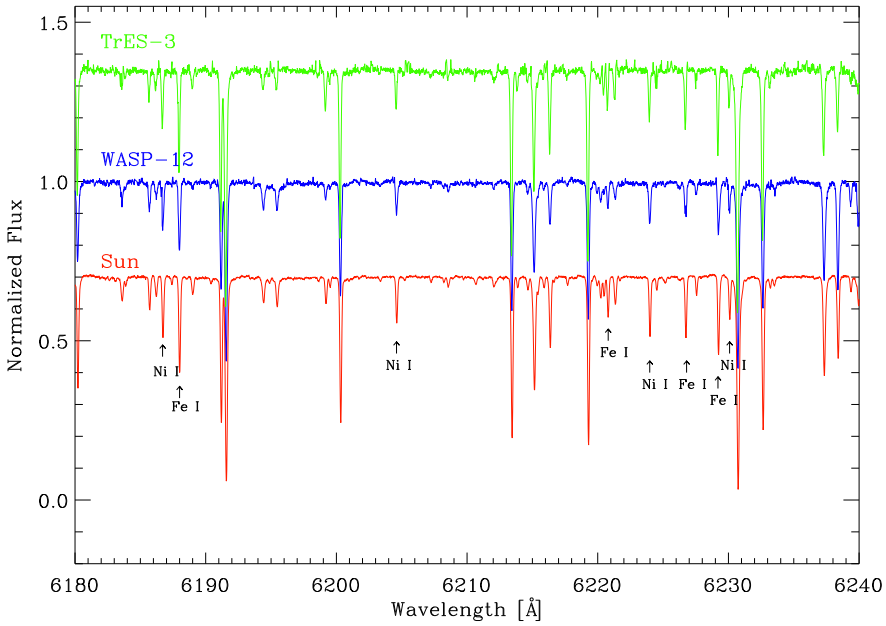

Fig. 1.— Sample spectra of TrES-3 (green), WASP-12 (blue), and the Sun (red) obtained with Subaru/HDS. The spectra have been continuum normalized and are shifted by constant values in flux for ease of viewing. Lines in this order for which EWs were measured are marked with arrows.

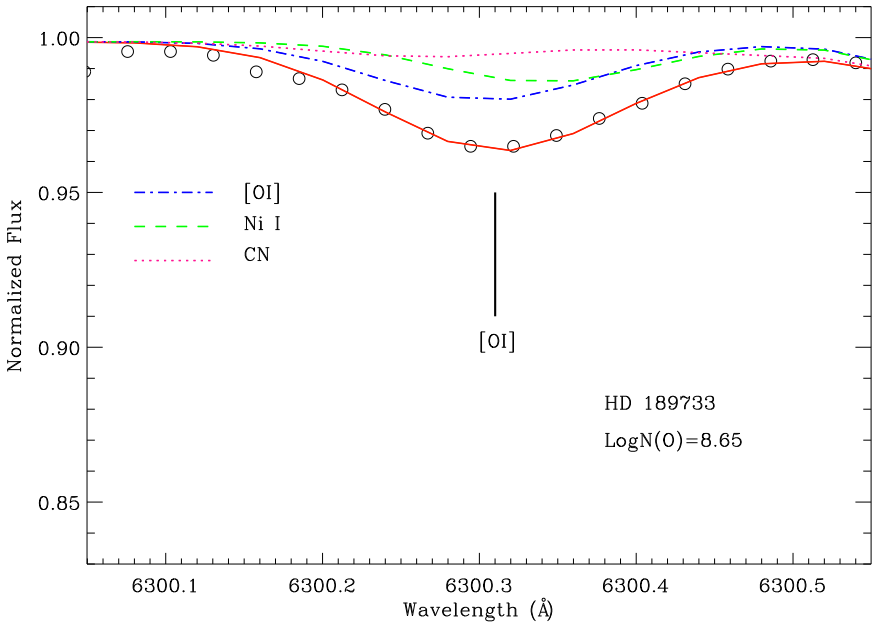

Fig. 2.— Shown here is the spectrum synthesis fit to the forbidden [OI] line (6300.3 {AA) for HD 189733. The data are shown as black open circles. The full synthesis fit is represented by a solid red line, with components shown with blue dash-dotted ([OI]), green dashed (Ni I), and pink dotted (CN) lines.

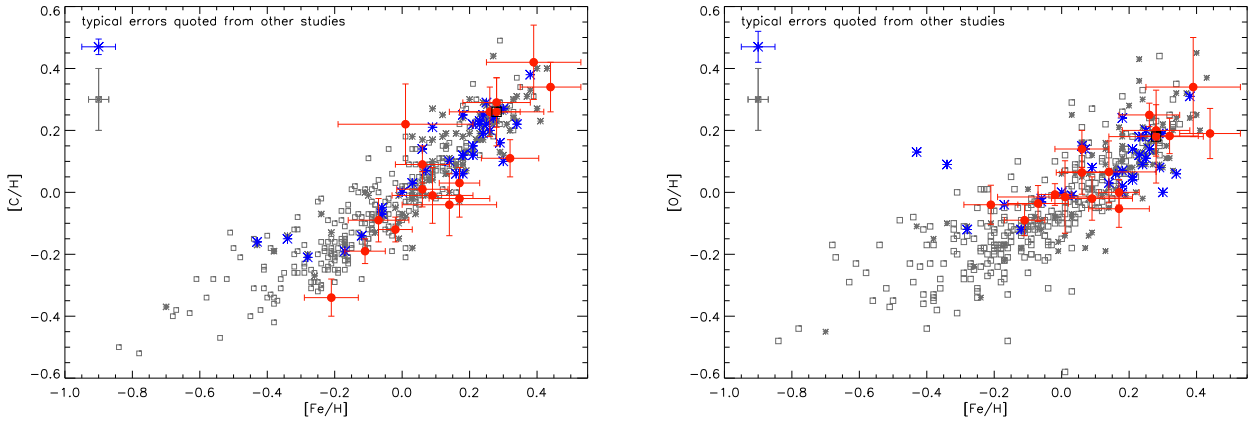

Fig. 3.— [C/H] and [O/H] versus [Fe/H] from Delgado Mena et al. (2010) and Nissen (2013) [all Nissen (2013) hosts are in the Delgado Mena et al. (2010) host sample]. Non-host stars from Delgado Mena et al. (2010) are plotted with gray open squares, while host stars from Delgado Mena et al. (2010)/Nissen (2013) are plotted with gray/blue asterisks. Quoted typical error bars are in the upper left. Measurements from this work are plotted as red filled circles, with error bars included (see Table 6). In particular, XO-2S is plotted as a red circle enclosed by a black square, to indicate that it does not host a known planet (in the C/O plot, XO-2N overlaps XO-2S).

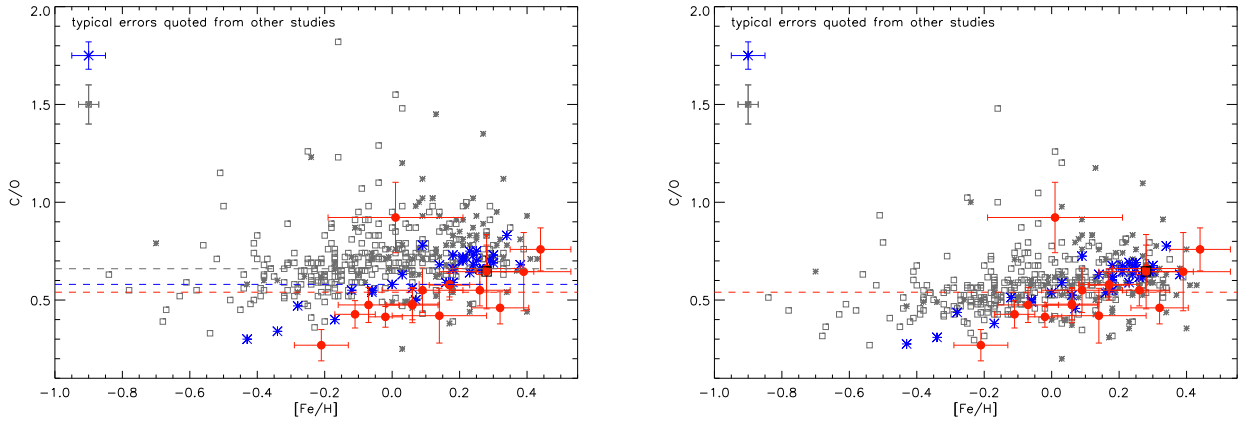

Fig. 4.— C/O versus [Fe/H] from Delgado Mena et al. (2010) and Nissen (2013) [all Nissen (2013) hosts are in the Delgado Mena et al. (2010) host sample]. Colors and symbols are the same as in Figure 3. Left: C/O ratios as reported in respective sources, using their $C/O_{\odot}$ (see text for discussion). Dashed lines show the $C/O_{\odot}$ adopted by each source. Right: All C/O ratios normalized to the same $C/O_{\odot}$ adopted in this work, $C/O_{\odot}$=0.54 ($\log N(C)_{\odot}$=8.39, $\log N(O)_{\odot}$=8.66; Asplund et al. 2005).

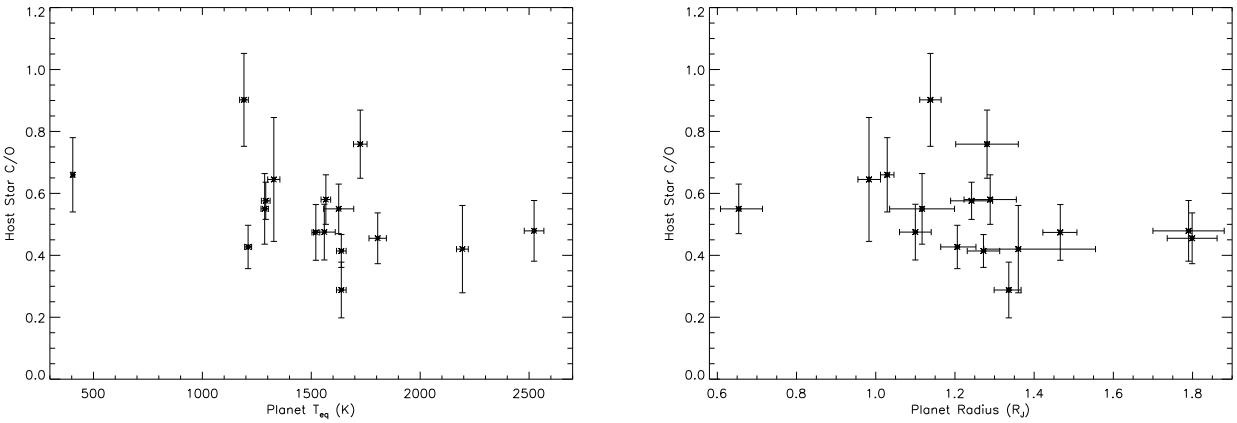

Fig. 5.— Host star C/O ratio versus planetary equilibrium temperature (left) and radius (right). The planetary parameters are from the NASA Exoplanet Archive, and the host star C/O ratios are derived in this paper.